

Serveur Académique Lausannois SERVAL serval.unil.ch

Author Manuscript

Faculty of Biology and Medicine Publication

This paper has been peer-reviewed but does not include the final publisher proof-corrections or journal pagination.

Published in final edited form as:

Title: Inhibition of cell migration and invasion mediated by the TAT-RasGAP317-326 peptide requires the DLC1 tumor suppressor.

Authors: Barras D, Lorusso G, Rüegg C, Widmann C

Journal: Oncogene

Year: 2014 Oct 30

Volume: 33

Issue: 44

Pages: 5163-72

DOI: 10.1038/onc.2013.465

In the absence of a copyright statement, users should assume that standard copyright protection applies, unless the article contains an explicit statement to the contrary. In case of doubt, contact the journal publisher to verify the copyright status of an article.

**Inhibition of cell migration and invasion mediated by the TAT-RasGAP₃₁₇₋₃₂₆ peptide requires the
DLC1 tumor suppressor**

David Barras¹, Gireca Lorusso², Curzio Rüegg², Christian Widmann¹

¹Department of Physiology, University of Lausanne, Switzerland and ²Department of Medicine, University
of Fribourg, Switzerland

Correspondence to Christian Widmann, Department of Physiology, Bugnon 7, 1005 Lausanne,
Switzerland, Phone: +41216925123, Fax: +41216925505, E-mail: Christian.Widmann@unil.ch.

Financial support: Oncosuisse (KFS-02543-02-2010)

Running title: TAT-RasGAP₃₁₇₋₃₂₆ inhibits migration and invasion

ABSTRACT

TAT-RasGAP₃₁₇₋₃₂₆, a peptide corresponding to the 317-326 sequence of p120 RasGAP coupled to a cell-permeable TAT-derived peptide, sensitizes the death response of various tumor cells to several anticancer treatments. We now report that this peptide is also able to increase cell adherence, prevent cell migration and inhibit matrix invasion. This is accompanied by marked modification of the actin cytoskeleton and focal adhesion redistribution. Interestingly, integrins and the small Rho GTP-binding protein, which are well characterized proteins modulating actin fibers, adhesion, and migration, do not appear to be required for the pro-adhesive properties of TAT-RasGAP₃₁₇₋₃₂₆. On the other hand, deleted in liver cancer-1 (DLC1), a tumor suppressor protein, the expression of which is often deregulated in cancer cells, was found to be required for TAT-RasGAP₃₁₇₋₃₂₆ to promote cell adherence and inhibit migration. These results show that TAT-RasGAP₃₁₇₋₃₂₆, besides its ability to favor tumor cell death, hampers cell migration and invasion.

KEYWORDS

RasGAP; DLC1; adhesion; migration; invasion; peptide

INTRODUCTION

Cancer is the second leading cause of mortality worldwide ¹. A hallmark of tumor cells is their ability to acquire an invasive phenotype and metastasize from the primary tumor ². Metastasis accounts for more than 90% of cancer-related death ^{1,2}. Metastatic dissemination begins with a cellular reprogramming that allows tumor cells to escape from the primary tumor, and that resumes with a long migration journey through tissues and in the vascular and lymphatic circulation ^{3,4}. Metastatic cells are characterized by their ability to degrade the extracellular matrix at the primary site and the new colonization site, and to undergo intravasation and extravasation into or from the blood and/or lymph vessels ⁵. Although the molecular events during the metastatic cascade are now relatively well understood, there are not yet tools to effectively inhibit critical steps of the metastatic cascade, and eventually metastasis formation ⁶.

A hallmark of metastatic progression and invasiveness is increased cell motility ^{7,8}. Cell migration is a complex multistep and spatiotemporally organized process. It involves the integration of signals that define cell polarity, dynamic remodeling of cytoskeleton and focal adhesion (FA) structures as well as the regulation of the adhesive interaction with the extracellular environment ⁸. FAs are structures that link the exterior of the cell to the cytoskeleton through integrin transmembrane proteins. On one hand, FAs allow the cells to anchor on its extracellular matrix and, on the other hand, they modulate various signaling event involved in cell migration ⁹. Small GTPases of the Rho family, in particular RhoA, Rac1 and Cdc42, are typically triggered by integrin engagement and finely coordinate cell migration at all levels ¹⁰. As an example, in addition to their central function on actin dynamics regulation, Rac1 and RhoA trigger FA formation and maturation, respectively ¹¹. Any impairment in these steps can result in an inefficient motility and therefore can compromise metastatic progression. From a therapeutic point of view, inhibiting cell migration is a logical approach for the development of anti-metastatic drugs since it is an early event in metastatic progression.

Dysregulation of pathways regulating actin cytoskeleton dynamics and cell migration is often required for cancer cell to attain their full oncogenic potential ⁷. This can be so crucial for tumor development that some proteins modulating these pathways are in fact tumor suppressors, such as neurofibromatosis type-2 (NF2) ¹² and adenomatous polyposis coli (APC) ¹³. One other such tumor suppressor is deleted in liver cancer-1 (DLC1), a RhoGAP protein acting on Rho and Cdc42 (ref. ¹⁴). DLC1 is mutated almost as often as p53

suggesting that it is a major player during cancer progression¹⁵. Its reintroduction in DLC1-negative cancer cells was reported to inhibit their tumorigenicity and invasive behavior in a Rho-dependent and Rho-independent manner¹⁶.

The *Rasa1* gene product p120 RasGAP (from now on referred to as RasGAP) is a negative modulator of the Ras small GTPase. RasGAP can also interact with a large number of other proteins via proline-rich, Src homology, pleckstrin homology, and C2 domains¹⁷. We previously reported that full cleavage of RasGAP by caspase-3 leads to the generation of fragment N2 (RasGAP₁₅₈₋₄₅₅) that efficiently and specifically sensitizes cancer cells to a panel of anticancer therapy-induced cell death¹⁸. The shortest region responsible for this effect resides in a 10-amino acid sequence (RasGAP₃₁₇₋₃₂₆) within the SH3 domain¹⁹. TAT-RasGAP₃₁₇₋₃₂₆ corresponds to this sequence hooked to a cell-permeable TAT-derived peptide and synthesized with D-amino acids. TAT-RasGAP₃₁₇₋₃₂₆ sensitizes a variety of tumor cells to genotoxin- and photodynamic therapy-induced death, both *in vitro* and *in vivo*^{19,20,21,22}. Importantly, it does not affect normal cells^{19,21}. In the present report, we show that TAT-RasGAP₃₁₇₋₃₂₆ increases cell adhesiveness and inhibits cell migration and invasion in a DLC1-dependent manner.

RESULTS

TAT-RasGAP₃₁₇₋₃₂₆ increases cell adhesiveness

By serendipity, we discovered that TAT-RasGAP₃₁₇₋₃₂₆ has a dramatic effect on cell adhesion to their substratum. Incubation of the U2OS human osteosarcoma cell line with TAT-RasGAP₃₁₇₋₃₂₆, but not with the TAT cell-permeable sequence alone, rendered it resistant to cell detachment by trypsin/EDTA in a time-dependent manner (Figure 1A). Three hours after incubation with the RasGAP-derived peptide, approximately 50% of the cells became resistant to detachment. The percentage of non-detachable cells increased to 90% after 8 hours of treatment. The TAT-RasGAP₃₁₇₋₃₂₆-induced resistance to trypsin/EDTA was also observed in seven other cancer and non-cancer cell lines (Figure 1B). This phenotype was found to be reversible 4 to 6 hours following removal of the peptide (Figure 1C). TAT-RasGAP₃₁₇₋₃₂₆ rendered U2OS cells resistant not only to trypsin-mediated detachment but also to EDTA-mediated detachment (Figure 1D). This indicates that the mechanism allowing TAT-RasGAP₃₁₇₋₃₂₆ to block cell detachment is not due to a potential inhibitory activity on trypsin. An adhesion assay was further performed to evaluate the effect of TAT-RasGAP₃₁₇₋₃₂₆ on adhesion speed (Figure 1E and Supplementary Figure S1A). It revealed that the RasGAP-peptide was not only negatively impinging on detachment but that it also significantly increased the cell adhesion rate. While the TAT peptide alone induced a statistically significant higher adhesion speed over untreated cells, TAT-RasGAP₃₁₇₋₃₂₆ stimulated an even faster cell adhesion rate. Of note, this adhesion was already detectable 30 minutes after the addition of the peptide but at this time point the cells have not acquired yet their ability to resist trypsin-mediated detachment (see Supplementary Figure S1B). TAT-RasGAP₃₁₇₋₃₂₆ treated cells displayed a spread phenotype in comparison with TAT and untreated cells (Supplementary Figure S1C). The increase in cell adhesion was confirmed using a flow-mediated detachment assay. Untreated and TAT-treated HeLa cells were detachable by a strong (400 μ l/s) and by a weaker (120 μ l/s) flow. In contrast, while TAT-RasGAP₃₁₇₋₃₂₆-treated cells were detachable by the strong flow, they remained adherent in the presence of the 120 μ l/s flow (Figure 2). These results indicate TAT-RasGAP₃₁₇₋₃₂₆ progressively increases cell adhesiveness and this is likely to be the cause of their resistance to cell detachment.

TAT-RasGAP₃₁₇₋₃₂₆ acts from within the cell

To start defining the mechanisms by which TAT-RasGAP₃₁₇₋₃₂₆ affects cell adhesion, we assessed the possibility that TAT-RasGAP₃₁₇₋₃₂₆ acts from the outside of the cells to induce its effect on cell adhesion. The RasGAP₃₁₇₋₃₂₆ peptide without the TAT cell-permeable sequence, which is therefore unable to efficiently penetrate cells, was unable to confer resistance to detachment (Supplementary Figure S2A) and to increase adhesion rate (Supplementary Figure S2B). Similar results were obtained by using another cell-permeable sequence, R9, a peptide composed of 9 arginine residues (Supplementary Figure S2A), indicating that the nature of the cell-permeable moiety attached to the RasGAP₃₁₇₋₃₂₆ sequence does not contribute to its activity on cell adhesion. Additionally, transfection of 293T cells with a plasmid encoding the RasGAP₃₁₇₋₃₂₆ sequence rendered cells resistant to trypsin-mediated detachment (Supplementary Figure S2C), demonstrating that cells can increase their adherence if they synthesize their own RasGAP₃₁₇₋₃₂₆ peptide. Interestingly, transfection of a plasmid encoding fragment N2 (RasGAP₁₅₈₋₄₅₅), the parental RasGAP-derived fragment generated by caspase-3 in apoptotic cells^{18,23}, also rendered cells resistant to detachment (Supplementary Figure S2C). This indicates that the peptide can be part of a larger polypeptide and still exerts its detachment resistance activity. These data provide new insights of a potential physiological function of fragment N2 that is generated upon high caspase-3 activity¹⁸. Taken together, these results suggest that TAT-RasGAP₃₁₇₋₃₂₆ triggers intracellular signaling pathways regulating cell adhesion.

TAT-RasGAP₃₁₇₋₃₂₆ mediates increased cell adherence through post-translational effects

Next, the requirement of transcription and translation for the capacity of TAT-RasGAP₃₁₇₋₃₂₆ to increase cell adhesion was evaluated. U2OS cells were treated with actinomycin D, to block transcription, or with cycloheximide, to block translation, and were then subjected to a trypsin-mediated detachment assay (Supplementary Figure S3A). These drugs efficiently inhibited transcription and translation as assessed by the disappearance of the short-lived c-Myc protein (Supplementary Figure S3A). In these conditions, TAT-RasGAP₃₁₇₋₃₂₆ was still able to increase adherence, indicating that the peptide acts post-translationally. The involvement of the proteasome was then tested. As shown in Supplementary Figure S3B (upper graph), the MG-132 proteasome inhibitor did not affect the capacity of TAT-RasGAP₃₁₇₋₃₂₆ to prevent cell detachment

despite being able to inhibit cycloheximide-induced c-Myc degradation (Supplementary Figure S3B; lower blot). The observation that staurosporine, a compound able to inhibit ~ 90% of all kinases ²⁴, did not affect TAT-RasGAP₃₁₇₋₃₂₆-induced increased adhesiveness (Supplementary Figure S3C), indicates that most kinases are not mediating the effect of the RasGAP-derived peptide. The RasGAP SH3 domain that harbors the RasGAP₃₁₇₋₃₂₆ sequence has the potential to dimerize ²⁵ raising the possibility that TAT-RasGAP₃₁₇₋₃₂₆ interacts with RasGAP or RasGAP-derived fragments and that such interaction is required for the peptide to render cells resistant to detachment. However, RasGAP knock-out mouse embryonic fibroblasts (MEFs) became resistant to trypsin-mediated detachment when incubated with TAT-RasGAP₃₁₇₋₃₂₆ (Supplementary Figure S3D). Therefore, the RasGAP-derived peptide does not require the endogenous wild-type molecule (i.e. RasGAP) to mediate its cellular effects on adhesion.

Integrins and CD44 adhesion receptors are not required for TAT-RasGAP₃₁₇₋₃₂₆-mediated increased cell adhesiveness

We investigated whether TAT-RasGAP₃₁₇₋₃₂₆ requires integrin functions. Integrins are heterodimers composed of one α and one β subunit. There are 18 different known α and β subunits that can combine to form 24 different heterodimers ⁹. About 70% (16 out of 24) of these integrin dimers are made of either the α_v - or the $\beta 1$ -integrins (Supplementary Figure S4A). The fact that a melanoma cell line deficient in α_v -integrin expression ²⁶ was rendered more adherent by TAT-RasGAP₃₁₇₋₃₂₆ (Supplementary Figure S4B) together with the observation that $\beta 1$ integrin silencing in HeLa cells did not prevent TAT-RasGAP₃₁₇₋₃₂₆ from triggering adherence (Supplementary Figure S4C) suggest however that these widespread integrins do not individually mediate the pro-adhesive phenotype induced by TAT-RasGAP₃₁₇₋₃₂₆. It is unlikely that other integrins are targeted by the RasGAP peptide to mediate its effects on adhesion for the following reasons: (i) $\beta 2$ -, $\beta 3$ -, $\beta 4$ -, $\beta 7$ -integrins are expressed at very low levels or are not detected in U2OS cells (Supplementary Figure S4D) ²⁷, which are cells that are responsive to TAT-RasGAP₃₁₇₋₃₂₆. (ii) $\beta 2$ - and $\beta 7$ -integrin expression is usually restricted to immune cells ²⁸. We also tested the involvement of the CD44 glycoprotein, a focal adhesion-independent adhesion receptor that can also interact with ECM ²⁹. However, upon CD44 silencing in HeLa cells, TAT-RasGAP₃₁₇₋₃₂₆ could still increase adhesion (Supplementary Figure S4E). Consistent with our results on integrins are the data showing that TAT-RasGAP₃₁₇₋₃₂₆-

mediated adhesion does not occur through a specific ECM since cell adhesion to collagen, fibronectin and laminin was increased by the RasGAP peptide (Supplementary Figure S4F). Altogether the results indicate that, CD44, β 1-integrin and α_v -integrin are individually dispensable for the adhesion-activating effect of TAT-RasGAP₃₁₇₋₃₂₆.

TAT-RasGAP₃₁₇₋₃₂₆ remodels focal adhesions and induces actin depolymerization

FAs are protein complexes through which the cytoskeleton is connected to the extracellular matrix and as such could be modulated by TAT-RasGAP₃₁₇₋₃₂₆ to increase cell adhesion. Focal adhesion kinase (FAK), when recruited to activated integrins, acts as a key protein during FA formation and turnover. For example, it regulates the dynamic of actin fibers by favoring actin polymerization through phosphorylation of N-WASP, actin contraction via activation of p190 RhoGEF, and actin fiber fluidity by phosphorylating α -actinin and inhibiting its actin cross-linking capacity³⁰. Even though FAK-null cells are still able to form FAs, FAK recruitment to integrins remains a typical feature of FA formation and subsequent attachment to the actin cytoskeleton^{30,31}. To assess FA modulation and actin polymerization upon TAT-RasGAP₃₁₇₋₃₂₆ treatment, U2OS cells were labeled with antibodies specific for FAK, phospho-Tyr³⁹⁷-FAK or stained for filamentous actin (F-actin). A marked increase in cortical actin fibers forming peripheral concentric arc-like structures (Figure 3A; white arrows) was induced by the RasGAP-derived peptide, while stress fibers almost completely disappeared (Figure 3A; yellow arrows). Unexpectedly, the overall number of FAs decreased and there was a redistribution of FAs to the cell periphery. In addition TAT-RasGAP₃₁₇₋₃₂₆ treatment resulted in significant dephosphorylation of FAK at tyrosine 397, which indicates a reduction in FA turnover³². Expression levels of the focal adhesion-associated FAK and vinculin proteins, or the cytoskeletal β -actin and α -tubulin, were not affected by the RasGAP-derived peptide (Figure 3B). The α -tubulin network was also not affected by TAT-RasGAP₃₁₇₋₃₂₆ (data not shown). Figure 3C shows that, using FAK knock-out MEFs, the absence of FAK did not prevent TAT-RasGAP₃₁₇₋₃₂₆ to increase adherence, excluding FAK as being the target of the RasGAP-derived peptide.

Because TAT-RasGAP₃₁₇₋₃₂₆-treated cells exhibited a loss of stress fibers, the effect of the peptide on actin fiber dynamics was investigated by measuring the ratio between polymerized F-actin and monomeric G-actin. Figure 4A shows that the F-/G-actin ratio was significantly decreased upon TAT-RasGAP₃₁₇₋₃₂₆

treatment to values similar as those obtained when known actin inhibitors (latrunculin A and cytochalasin D) were used. Interestingly, like TAT-RasGAP₃₁₇₋₃₂₆, both latrunculin A and cytochalasin D increased cell adhesion while jasplakinolide, an actin polymerization inducer, did not (Figure 4B). This suggests that actin depolymerization is involved in TAT-RasGAP₃₁₇₋₃₂₆-mediated cell adhesion increase. An *in vitro* pyrene-actin-based polymerization assay revealed however that RasGAP₃₁₇₋₃₂₆ alone does not slow down actin polymerization (Figure 4C), indicating that TAT-RasGAP₃₁₇₋₃₂₆-mediated actin depolymerization in cells is indirect.

TAT-RasGAP₃₁₇₋₃₂₆ does not require the Rho/ROCK axis to increase cell adhesiveness

As the SH3 domain of RasGAP has been shown to remodel the actin cytoskeleton in a Rho-dependent manner³³, we investigated whether the activity of Rho could be modulated by the RasGAP-derived peptide. The level of the active GTP-bound RhoA, the main Rho family member, was assessed by performing a pull-down assay using the Rho-binding domain (RBD) of the Rhotekin protein that specifically binds to GTP-RhoA³⁴. TAT-RasGAP₃₁₇₋₃₂₆-pretreated cells exhibited significantly higher peak of Rho activation after 1 minute of serum exposure (Figure 5A). These results show that, albeit only transiently, TAT-RasGAP₃₁₇₋₃₂₆ modulates Rho activation. RasGAP and p190RhoGAP have been previously reported to form a complex, the biological relevance of which is thought to coordinate Ras and Rho-mediated signaling pathways³⁵. The possibility that TAT-RasGAP₃₁₇₋₃₂₆ disrupts this complex was evaluated. Supplementary Figure S5 shows that the RasGAP-RhoGAP interaction was not modulated by the RasGAP peptide, suggesting that the increase in RhoA activity by TAT-RasGAP₃₁₇₋₃₂₆ was not modulated at this level. This result is also consistent with the fact that the RasGAP-derived peptide does not require full-length RasGAP to mediate its effects (see Supplementary Figure S3D).

To further understand if the TAT-RasGAP₃₁₇₋₃₂₆-mediated transient RhoA activation was needed for the increase in cell adherence, a trypsin-mediated detachment assay was performed in the absence or in the presence of the *Botulinum* C3 exoenzyme Rho inhibitor or Y-27632, an inhibitor of ROCK, an effector of Rho. Treatment with both drugs did not prevent TAT-RasGAP₃₁₇₋₃₂₆ from increasing adherence, indicating that TAT-RasGAP₃₁₇₋₃₂₆ does not mediate adhesion increase through activation of the Rho-ROCK pathway

(Figure 5B). TAT-RasGAP₃₁₇₋₃₂₆ also prevented cell shrinking/rounding induced by the C3 exoenzyme (Figure 5C), a possible consequence of its capacity to increase adhesiveness.

TAT-RasGAP₃₁₇₋₃₂₆ impairs cell migration and invasion

It has been reported that a strong adhesion of cells to their substratum correlates with poor migration³⁶. These observations raise the possibility that TAT-RasGAP₃₁₇₋₃₂₆ affects cell migration. Scratch wound healing assays were used to evaluate this assumption. Four different cancer and non-cancer cell lines (U2OS, HCT116, HeLa and HaCaT) were wounded and simultaneously treated or not with the peptides. A 48 hour period of time was sufficient for untreated and TAT-only treated cells to fill the wounds entirely, whereas TAT-RasGAP₃₁₇₋₃₂₆-treated cells exhibited highly impaired motility (Figure 6A; time-lapse movie in supplementary material). This observation was further confirmed using a transwell Boyden chamber migration assay in which TAT-RasGAP₃₁₇₋₃₂₆ recapitulated the inhibition on cell migration (Figure 6B). Because RasGAP modulates cell proliferation through Ras, we assessed if TAT-RasGAP₃₁₇₋₃₂₆ affects cell proliferation to rule out the possibility that impaired migration was a consequence of decreased proliferation. However, the peptide did not impair proliferation of adherent cells (Supplementary Figure S6A) or cells in suspension (Supplementary Figure S6B). These results were confirmed by testing the ability of U2OS cells to incorporate radioactive thymidine in the presence of TAT-RasGAP₃₁₇₋₃₂₆ (Supplementary Figure S6C). As migration is a hallmark of invasiveness, we tested whether TAT-RasGAP₃₁₇₋₃₂₆ could hamper cell invasion. Using a transwell Boyden chamber, it was found that TAT-RasGAP₃₁₇₋₃₂₆ also prevented invasion of MDA-MB-231 cells into basement membrane matrix (Figure 6C).

DLC1 is required for TAT-RasGAP₃₁₇₋₃₂₆-mediated migration inhibition

Several RasGAP binding partners have been identified in the past¹⁷. Among them, DLC1, a RhoGAP with tumor and metastasis suppressor activities, binds the SH3 domain of RasGAP via its GAP domain^{14,37}. The reported consequence of this binding is an inhibition of the DLC1 RhoGAP activity and impairment of its oncosuppressive activity. Fragment N2, the RasGAP₃₁₇₋₃₂₆-containing polypeptide that is physiologically

generated by high levels of caspase-3²³ and that increases cell adhesion (Supplementary Figure S2C) was also able to interact with DLC1 (Figure 7A). However, an alanine substitution of tryptophan 317, an evolutionary conserved residue within the RasGAP₃₁₇₋₃₂₆ sequence, abrogated the ability of fragment N2 to bind to DLC1 (Figure 7A). A TAT-RasGAP₃₁₇₋₃₂₆ peptide version bearing the W317A mutation failed to increase cell adherence (Figure 7B). These results indicate that the interaction of tryptophan 317 with DLC1 is essential for TAT-RasGAP₃₁₇₋₃₂₆-mediated effects on cell adhesiveness.

The involvement of DLC1 in the pro-adhesion and anti-migratory functions of TAT-RasGAP₃₁₇₋₃₂₆ was assessed in DLC1 knock-out MEFs. In contrast to wild-type MEFs, DLC1-null MEFs were efficiently detached by trypsin despite the presence of TAT-RasGAP₃₁₇₋₃₂₆, (Figure 7C) Moreover, TAT-RasGAP₃₁₇₋₃₂₆ did not, or only minimally, hamper migration of DLC1-null cells, in contrast again to wild-type MEFs that were unable to migrate into wounds in the presence of the peptide (Figure 7D). To exclude the possibility that the inability of the DLC1 knock-out MEFs to respond to TAT-RasGAP₃₁₇₋₃₂₆ was caused by something else than the absence of DLC1, the DLC1-null cells were transfected with a DLC1-encoding plasmid together with a GFP-encoding plasmid to label and track the transfected cells. Figure 7E shows the transfected cells, in contrast to the non-transfected ones, were markedly impaired in the ability to migrate into wounds in the presence of TAT-RasGAP₃₁₇₋₃₂₆. Altogether these experiments demonstrate that the RasGAP-derived peptide requires DLC1 to exert its pro-adhesion and anti-migratory activities.

DISCUSSION

Blocking invasion is a prime strategy to inhibit the initial steps of the metastatic dissemination. In this study, we found that TAT-RasGAP₃₁₇₋₃₂₆, previously shown to sensitize cancer cells to various anticancer treatments^{19,20,21}, potently inhibits cell migration and invasion by targeting the DLC1 tumor suppressor.

Earlier reports have indicated that RasGAP can control cell migration. RasGAP knock-out MEFs exhibit reduced migration, while RasGAP silencing in breast cancer cells enhances their motility^{38,39}. These conflicting results could be a consequence of the different cellular systems investigated. Another possibility is that the dosage of RasGAP reduction influences the resulting effect on migration. It can be envisioned that RasGAP regulates both positively and negatively cell migration, possibly in response to different stimuli, but that the negative regulation requires high level of expression of the protein. In this case, reduction of RasGAP levels could favor cell migration. The observation that overexpression of RasGAP fragments correlates with decreased adherence⁴⁰ is consistent with this notion. In contrast, complete absence of RasGAP expression, as is the case in knock-out cells, would remove any positive effect of RasGAP on cell migration. However, the ability of TAT-RasGAP₃₁₇₋₃₂₆ to inhibit cell migration does not involve a modulation of the full-length RasGAP protein as the peptide also blocks cell migration in RasGAP knock-out cells (Supplementary Figure S3). It is therefore likely that if full-length RasGAP and TAT-RasGAP₃₁₇₋₃₂₆ use the same pathway to regulate cell adhesion, it is a consequence of targeting the same molecules and not the result of the peptide modulating the activity of the parental RasGAP protein.

The SH3 domain of RasGAP can reorganize actin cytoskeleton in a Rho-dependent manner^{33,38}, presumably via the recruitment of p190RhoGAP^{35,38}. TAT-RasGAP₃₁₇₋₃₂₆ can also favor Rho activation, at least transiently (Figure 5) but this apparently is not required for its capacity to increase cell adherence as inhibition of Rho or the Rho effector ROCK does not affect TAT-RasGAP₃₁₇₋₃₂₆-mediated cell adhesiveness increase.

Although α_v - and β_1 -integrins were not individually required, TAT-RasGAP₃₁₇₋₃₂₆ may nevertheless exert its effects through FA modulation. Rac-induced formation of nascent FAs can generate huge adhesive forces¹¹, raising the hypothesis that the RasGAP-derived peptide prevents FA maturation, therefore retaining FAs in their hyper-adherent state. Consistent with this hypothesis are the observations that TAT-RasGAP₃₁₇₋₃₂₆ induced FAK dephosphorylation and relocation of FAs to the cell periphery (Figure 3),

which is typical of FA turnover inhibition ¹¹. The involvement of other adhesion receptors in TAT-RasGAP₃₁₇₋₃₂₆-mediated adherence, such as syndecans and cell adhesion molecules (CAMs) remains to be investigated.

How can DLC1-dependent signaling increase adherence? The fact that DLC1 is located at FAs ⁴¹, where it binds tensin, talin and FAK ⁴², is certainly appropriate for a potential effect on adhesion and cell migration. DLC1 has indeed been shown to inhibit migration, both in Rho-dependent and Rho-independent ways ¹⁴. However, as mentioned above, the peptide seems to exert its effects even when Rho is inhibited indicating that the peptide triggers a Rho-independent DLC1-mediated signaling. Such signaling could involve the PLC δ 1 phospholipase. DLC1 binds to and positively regulates PLC δ 1, which results in PIP₂ hydrolysis ⁴³. PIP₂ activates actin polymerization through various mechanisms [reviewed in ⁴³] and its hydrolysis leads to actin depolymerization, a response indeed induced by TAT-RasGAP₃₁₇₋₃₂₆ (Figure 4). An attractive possibility is that TAT-RasGAP₃₁₇₋₃₂₆ by interacting with DLC-1 prevents the binding of the latter to PLC δ 1 thereby decreasing PLC δ 1 hydrolyzing activity and leading to actin depolymerization and inhibition of migration. This would also induce peripheral FA redistribution ³², a phenotype that is seen in TAT-RasGAP₃₁₇₋₃₂₆-treated cells (Figure 3). The fact that displacing DLC1 from FAs, through abrogation of FAK and tensin binding, does not affect DLC1 RhoGAP activity ⁴² is consistent with our observation that Rho activity is not modulated by TAT-RasGAP₃₁₇₋₃₂₆ (Figure 5).

DLC1 may not be the only target of the RasGAP-derived peptide as some residual attachment was observed in TAT-RasGAP₃₁₇₋₃₂₆-treated DLC1-null MEFs (Figure 7). For example, proteins sharing redundancy with DLC1, such as DLC2 and DLC3 may partially compensate for the lack of DLC1. The involvement of such proteins in TAT-RasGAP₃₁₇₋₃₂₆ functions remains to be investigated.

The present study identifies TAT-RasGAP₃₁₇₋₃₂₆ as an activator of cell adhesion and an inhibitor of cell migration and invasion. Earlier work has shown that this RasGAP-derived peptide increases the death of tumor cells induced by various anticancer treatments ^{19,20,21}. Therefore TAT-RasGAP₃₁₇₋₃₂₆ could exert two beneficial effects as an anticancer agent, first by increasing the sensitivity of tumor cells to anticancer drugs and second by reducing the invasive potential of tumor cells.

MATERIAL AND METHODS

Cell lines, cell culture and transfection

All cell lines were cultured at 37°C and in 5% CO₂. U2OS, 4T1, HCT116, SAOS, 3T3, RasGAP-null, FAK-null and DLC1-null mouse embryonic fibroblasts (MEFs), M21 (α_v -integrin null), M21L (α_v -integrin positive), MDA-MB-231-Luc and 293T cells were maintained in Dulbecco's modified Eagle Medium (DMEM) (Gibco; Paisley; UK) supplemented with 10% fetal bovine serum (FBS) (Gibco). HeLa and Jurkat cells were maintained in RPMI 1640 (Gibco) supplemented with 10% FBS. HaCaT cells were maintained in keratinocyte medium (Invitrogen; Carlsbad; CA; USA). The 293T cells were transfected using the calcium-phosphate method^{19,44}. MEFs were transfected using the Lipofectamine™ 2000 reagent (Invitrogen) according to the manufacturer's instructions.

Antibodies

The antibodies used were obtained from the following sources (their dilution and specific buffer are described in the supplementary methods): anti-c-Myc, anti-FAK, anti-phospho-Tyr³⁹⁷-FAK, and anti-RhoA (Cell Signaling; Danvers; MA; USA), anti-vinculin (Sigma-Aldrich; St-Louis; MO; USA), anti- β -actin (Chemicon; Billerica; MA; USA), anti- α -tubulin (Serotec; Raleigh; NC; USA), anti-RasGAP (Enzo life sciences; Farmingdale, NY; USA), anti-CD44 (Abcam; UK), anti- β 1-integrin (BD Pharmingen; San Jose; CA; USA), anti-V5 (Invitrogen), anti-HA (Covance; Princeton; NJ; USA). The secondary antibodies were IRDye800-conjugated anti-mouse IgG and IRDye800-conjugated anti-rabbit IgG (Rockland; Gilbertsville; PA; US), AlexaFluor680-conjugated anti-mouse IgG and AlexaFluor680-conjugated anti-rabbit IgG (Molecular Probes; UK) and donkey CyTM-anti-rabbit antibody (Jackson ImmunoResearch; West Grove; PA; USA; for immunocytochemistry).

Peptide synthesis and treatment, and plasmids

All peptides are described and were synthesized as previously reported¹⁹. The R9 and R9-RasGAP₃₁₇₋₃₂₆ peptides were kind gifts from Dr. Christoph Kündig (MedDiscovery, Switzerland). Plasmid description is detailed in the supplementary methods.

Detachment assay

Cells were cultured until 80% confluence and were treated as indicated in the figures. After a PBS wash, the non-trypsinized cells were directly colored with the Giemsa stain. The other cells were incubated with 5 g/l trypsin, 15 mM EDTA solution or with trypsin/EDTA (5 g/l trypsin, 6.8 mM EDTA) for 5 minutes. The cells were then washed once with PBS and colored with the Giemsa stain. Four pictures per plate were taken using a Zeiss Axioplan 2 microscope equipped with a 10 X objective. The number of adherent cells was then counted for each picture and expressed as the number of cells per mm² or alternatively as the percentage of adherent cells over the non-trypsinized control. The flow-mediated detachment assay is precisely described in the supplementary methods.

Adhesion assay

U2OS cells were let adhering with the indicated compounds and for the indicated period of time. The medium was then aspirated and the cells were gently washed once with PBS and colored with the Giemsa stain. The data were collected as for detachment assays.

Western blot analysis

Cells were treated as indicated in the figures and Western blots were performed as previously described¹⁹. Unless otherwise mentioned, forty µg of proteins were loaded.

Wound-healing scratch assay, transwell migration and invasion assays

Wound-healing scratch assays were performed as described earlier⁴⁵ and details are described in the supplementary methods. For the transwell migration assay, fifty thousand overnight starved 4T1 cells were seeded in the upper chamber of 24 transwell plates (Corning; NY; USA) for 2.5 hours. The cells were then subjected to the treatments indicated in the figures for 3 hours. DMEM medium complemented or not with 10% FBS was then placed in the lower chamber of the transwell plates and the cells were allowed to migrate for 24 hours. Cells that migrated through the filters were quantified as described in the supplementary methods.

For the transwell invasion assay, overnight starved MDA-MB-231-luc cells were pre-treated for 2 hours with 20 μ M TAT, 20 μ M TAT-RasGAP₃₁₇₋₃₂₆ or left untreated. Five thousand cells were resuspended in 100 μ l of 4 mg/ml Matrigel (BD Biosciences; San Jose; CA; USA) complemented or not with 20 μ M TAT, 20 μ M TAT-RasGAP₃₁₇₋₃₂₆, and placed in the top chamber. DMEM medium complemented or not with 10% FBS was then placed in the bottom chamber and the cells were allowed to migrate through the filter for 48 hours. The crystal-violet colored invading cells were then counted for each condition and the results were expressed as the percentage of invading cells per transwell over the "control + serum" condition.

Statistical analysis

Unless otherwise mentioned, all experiments were performed three times and independently. The results were always expressed as mean \pm 95% confidence intervals. Unless otherwise mentioned, Student's t-tests were performed to assess significant differences and using the appropriate Microsoft Excel function. The Bonferroni correction was applied when more than one comparison was performed. One-way and repeated measurement ANOVAs were performed using the R software (version 2.11.0) and were followed by a Tukey test for multiple comparisons. Asterisks denote statistical significant differences (p-value < 0.05).

CONFLICT OF INTEREST

CW is a co-inventor of the TAT-RasGAP₃₁₇₋₃₂₆ compound as an anti-tumor agent (patent owned by the University of Lausanne) and may receive royalties from patent licensing if the compound is commercialized.

ACKNOWLEDGMENTS

This work was supported by a grant from Oncosuisse (KFS-02543-02-2010). We thank Pr. Nicholas C. Popescu (National Cancer Institute, Bethesda) for the DLC1-null MEFs and Pr. David Schlaepfer (Moores UCSD Cancer Center, La Jolla) for the FAK-null MEFs.

References

- 1 Jemal A, Bray F, Center MM, Ferlay J, Ward E, and Forman D. Global cancer statistics. *CA Cancer J Clin* 2011; **61**(2): 69-90
- 2 Hanahan D and Weinberg RA. Hallmarks of cancer: the next generation. *Cell* 2011; **5**: 646-674
- 3 Thiery JP. Epithelial-mesenchymal transitions in tumour progression. *Nat Rev Cancer* 2002; **6**: 442-454
- 4 Yilmaz M and Christofori G. EMT, the cytoskeleton, and cancer cell invasion. *Cancer Metastasis Rev* 2009; **1-2**: 15-33
- 5 Chiang AC and Massague J. Molecular basis of metastasis. *N Engl J Med* 2008; **26**: 2814-2823
- 6 Sethi N and Kang Y. Unravelling the complexity of metastasis - molecular understanding and targeted therapies. *Nat Rev Cancer* 2011; **10**: 735-748
- 7 Bravo-Cordero JJ, Hodgson L, and Condeelis J. Directed cell invasion and migration during metastasis. *Curr Opin Cell Biol* 2012; **2**: 277-283
- 8 Friedl P and Wolf K. Tumour-cell invasion and migration: diversity and escape mechanisms. *Nat Rev Cancer* 2003; **5**: 362-374
- 9 Byron A, Morgan MR, and Humphries MJ. Adhesion signalling complexes. *Curr Biol* 2010; **24**: R1063-R1067
- 10 Raftopoulou M and Hall A. Cell migration: Rho GTPases lead the way. *Dev Biol* 2004; **1**: 23-32
- 11 Geiger B, Bershadsky A, Pankov R, and Yamada KM. Transmembrane crosstalk between the extracellular matrix--cytoskeleton crosstalk. *Nat Rev Mol Cell Biol* 2001; **11**: 793-805
- 12 McClatchey AI and Giovannini M. Membrane organization and tumorigenesis--the NF2 tumor suppressor, Merlin. *Genes Dev* 2005; **19**: 2265-2277
- 13 Aoki K and Taketo MM. Adenomatous polyposis coli (APC): a multi-functional tumor suppressor gene. *J Cell Sci* 2007; **Pt 19**: 3327-3335
- 14 Durkin ME, Yuan BZ, Zhou X, Zimonjic DB, Lowy DR, Thorgeirsson SS *et al.* DLC-1: a Rho GTPase-activating protein and tumour suppressor. *J Cell Mol Med* 2007; **5**: 1185-1207
- 15 Lahoz A and Hall A. DLC1: a significant GAP in the cancer genome. *Genes Dev* 2008; **13**: 1724-1730
- 16 Yang X, Popescu NC, and Zimonjic DB. DLC1 interaction with S100A10 mediates inhibition of in vitro cell invasion and tumorigenicity of lung cancer cells through a RhoGAP-independent mechanism. *Cancer Res* 2011; **8**: 2916-2925
- 17 Pamonsinlapatham P, Hadj-Slimane R, Lepelletier Y, Allain B, Toccafondi M, Garbay C *et al.* P120-Ras GTPase activating protein (RasGAP): a multi-interacting protein in downstream signaling. *Biochimie* 2009; **3**: 320-328
- 18 Yang JY and Widmann C. Antiapoptotic signaling generated by caspase-induced cleavage of RasGAP. *Mol Cell Biol* 2001; **16**: 5346-5358

- 19 Michod D, Yang JY, Chen J, Bonny C, and Widmann C. A RasGAP-derived cell permeable peptide potently enhances genotoxin-induced cytotoxicity in tumor cells. *Oncogene* 2004; **55**: 8971-8978
- 20 Michod D, Annibaldi A, Schaefer S, Dapples C, Rochat B, and Widmann C. Effect of RasGAP N2 fragment-derived peptide on tumor growth in mice. *J Natl Cancer Inst* 2009; **11**: 828-832
- 21 Pittet O, Petermann D, Michod D, Krueger T, Cheng C, Ris HB *et al.* Effect of the TAT-RasGAP(317-326) peptide on apoptosis of human malignant mesothelioma cells and fibroblasts exposed to meso-tetra-hydroxyphenyl-chlorin and light. *J Photochem Photobiol B* 2007; **1**: 29-35
- 22 Barras D and Widmann C. Promises of apoptosis-inducing peptides in cancer therapeutics. *Curr Pharm Biotechnol* 2011; **8**: 1153-1165
- 23 Yang JY, Walicki J, Michod D, Dubuis G, and Widmann C. Impaired Akt activity down-modulation, caspase-3 activation, and apoptosis in cells expressing a caspase-resistant mutant of RasGAP at position 157. *Mol Biol Cell* 2005; **8**: 3511-3520
- 24 Karaman MW, Herrgard S, Treiber DK, Gallant P, Atteridge CE, Campbell BT *et al.* A quantitative analysis of kinase inhibitor selectivity. *Nat Biotechnol* 2008; **1**: 127-132
- 25 Ross B, Kristensen O, Favre D, Walicki J, Kastrup JS, Widmann C *et al.* High resolution crystal structures of the p120 RasGAP SH3 domain. *Biochem Biophys Res Commun* 2007; **2**: 463-468
- 26 Felding-Habermann B, Mueller BM, Romerdahl CA, and Cheresch DA. Involvement of integrin alpha V gene expression in human melanoma tumorigenicity. *J Clin Invest* 1992; **6**: 2018-2022
- 27 Beck M, Schmidt A, Malmstroem J, Claassen M, Ori A, Szymborska A *et al.* The quantitative proteome of a human cell line. *Mol Syst Biol* 2011; **7**: 549
- 28 Sheppard D. In vivo functions of integrins: lessons from null mutations in mice. *Matrix Biol* 2000; **3**: 203-209
- 29 Ponta H, Sherman L, and Herrlich PA. CD44: from adhesion molecules to signalling regulators. *Nat Rev Mol Cell Biol* 2003; **1**: 33-45
- 30 Mitra SK, Hanson DA, and Schlaepfer DD. Focal adhesion kinase: in command and control of cell motility. *Nat Rev Mol Cell Biol* 2005; **1**: 56-68
- 31 Ilic D, Furuta Y, Kanazawa S, Takeda N, Sobue K, Nakatsuji N *et al.* Reduced cell motility and enhanced focal adhesion contact formation in cells from FAK-deficient mice. *Nature* 1995; **6549**: 539-544
- 32 Hamadi A, Bouali M, Dontenwill M, Stoeckel H, Takeda K, and Ronde P. Regulation of focal adhesion dynamics and disassembly by phosphorylation of FAK at tyrosine 397. *J Cell Sci* 2005; **Pt 19**: 4415-4425
- 33 Leblanc V, Tocque B, and Delumeau I. Ras-GAP controls Rho-mediated cytoskeletal reorganization through its SH3 domain. *Mol Cell Biol* 1998; **9**: 5567-5578
- 34 Ren XD, Kiosses WB, and Schwartz MA. Regulation of the small GTP-binding protein Rho by cell adhesion and the cytoskeleton. *EMBO J* 1999; **3**: 578-585
- 35 Hu KQ and Settleman J. Tandem SH2 binding sites mediate the RasGAP-RhoGAP interaction: a conformational mechanism for SH3 domain regulation. *EMBO J* 1997; **3**: 473-483

- 36 Palecek SP, Loftus JC, Ginsberg MH, Lauffenburger DA, and Horwitz AF. Integrin-ligand binding properties govern cell migration speed through cell-substratum adhesiveness. *Nature* 1997; **6616**: 537-540
- 37 Yang XY, Guan M, Vigil D, Der CJ, Lowy DR, and Popescu NC. p120Ras-GAP binds the DLC1 Rho-GAP tumor suppressor protein and inhibits its RhoA GTPase and growth-suppressing activities. *Oncogene* 2009; **11**: 1401-1409
- 38 Kulkarni SV, Gish G, van der Geer P, Henkemeyer M, and Pawson T. Role of p120 Ras-GAP in directed cell movement. *J Cell Biol* 2000; **2**: 457-470
- 39 Mai A, Veltel S, Pellinen T, Padzik A, Coffey E, Marjomaki V *et al.* Competitive binding of Rab21 and p120RasGAP to integrins regulates receptor traffic and migration. *J Cell Biol* 2011; **2**: 291-306
- 40 McGlade J, Brunkhorst B, Anderson D, Mbamalu G, Settleman J, Dedhar S *et al.* The N-terminal region of GAP regulates cytoskeletal structure and cell adhesion. *EMBO J* 1993; **8**: 3073-3081
- 41 Kawai K, Yamaga M, Iwamae Y, Kiyota M, Kamata H, Hirata H *et al.* A PLCdelta1-binding protein, p122RhoGAP, is localized in focal adhesions. *Biochem Soc Trans* 2004; **Pt 6**: 1107-1109
- 42 Li G, Du X, Vass WC, Papageorge AG, Lowy DR, and Qian X. Full activity of the deleted in liver cancer 1 (DLC1) tumor suppressor depends on an LD-like motif that binds talin and focal adhesion kinase (FAK). *Proc Natl Acad Sci U S A* 2011; **41**: 17129-17134
- 43 Yin HL and Janmey PA. Phosphoinositide regulation of the actin cytoskeleton. *Annu Rev Physiol* 2003; **65**: 761-789
- 44 Jordan M, Schallhorn A, and Wurm FM. Transfecting mammalian cells: optimization of critical parameters affecting calcium-phosphate precipitate formation. *Nucleic Acids Res* 1996; **4**: 596-601
- 45 Bulat N, Waeber G, and Widmann C. LDLs stimulate p38 MAPKs and wound healing through SR-BI independently of Ras and PI3 kinase. *J Lipid Res* 2009; **1**: 81-89

FIGURE LEGENDS

Figure 1. TAT-RasGAP₃₁₇₋₃₂₆ induces cell adhesion.

A. U2OS cells were treated or not for the indicated periods of time with 20 μ M TAT or TAT-RasGAP₃₁₇₋₃₂₆ and were subjected to a trypsin-based detachment assay. Representative images of the cells remaining attached to the plates after trypsin treatment are shown on top of the panel. Scale bar: 100 μ m.

B. The indicated cell lines were left untreated or incubated for 8 hours with 20 μ M TAT or TAT-RasGAP₃₁₇₋₃₂₆, and then subjected to a trypsin-based detachment assay. Values too low to be seen on the figure graphs are shown literally.

C. Reversibility of the trypsin-mediated detachment induced by TAT-RasGAP₃₁₇₋₃₂₆. U2OS cells were left untreated or incubated during 24 hours with 20 μ M TAT or TAT-RasGAP₃₁₇₋₃₂₆. The cells were then washed twice with PBS and further incubated for the indicated periods of time in fresh culture medium, followed by a trypsin-based detachment assay.

D. TAT-RasGAP₃₁₇₋₃₂₆ prevents EDTA-only- and trypsin-only-mediated cell detachment. U2OS cells were treated for 8 hours with 20 μ M TAT, TAT-RasGAP₃₁₇₋₃₂₆ or left untreated. The cells were then subjected to an EDTA- and trypsin-based detachment assay (n=4 independent experiments). Values too low to be seen on the figure graphs are shown literally.

E. U2OS cells were subjected to an adhesion assay in presence of 20 μ M TAT or TAT-RasGAP₃₁₇₋₃₂₆ or without treatment (the statistical significance of the observed differences was assessed by one-way ANOVA).

Figure 2. TAT-RasGAP₃₁₇₋₃₂₆ increases anchorage strength of cells to their substratum.

HeLa cells were plated on gelatin-coated coverslips and were treated for 16 hours with 20 μ M TAT, TAT-RasGAP₃₁₇₋₃₂₆ or left untreated. They were then subjected to a flow-mediated detachment assay. The images shown are representative and display the cells after a detachment provoked by an intermediate strength flow (120 μ l/s) or by an intense flow (400 μ l/s). Scale bar: 100 μ m.

Figure 3. TAT-RasGAP₃₁₇₋₃₂₆ remodels actin cytoskeleton and focal adhesions.

A. U2OS cells were treated 16 hours with 20 μ M TAT, TAT-RasGAP₃₁₇₋₃₂₆ or left untreated. Immunohistochemistry staining against FAK and its phosphorylated form on tyrosine 397 (in red) was then performed. The F-actin cytoskeleton was stained with fluorescent phalloidin (in green) and nuclei were stained with Hoechst-33342 (in blue). Yellow arrows point at stress fibers and white arrows at cortical actin fibers. Scale bar: 10 μ m.

B. U2OS cells were treated 16 hours with 20 μ M TAT, TAT-RasGAP₃₁₇₋₃₂₆ (TAT-P) or left untreated (Ctrl). The expression of the indicated proteins was assessed by Western blotting. Representative images and quantitations are shown (n=6 independent experiments).

C. Wild-type MEFs or FAK^{-/-} MEFs were treated for 8 hours with 20 μ M TAT, TAT-RasGAP₃₁₇₋₃₂₆ or left untreated and a trypsin-mediated detachment assay was performed. FAK expression was checked by immunoblotting. Values too low to be seen on the figure graphs are shown literally.

Figure 4. TAT-RasGAP₃₁₇₋₃₂₆ depolymerizes actin and actin depolymerization-inducing agents increase adherence.

A. U2OS cells were treated for 16 hours with 50 nM of the actin polymerization promoter jasplakinolide (Jasp), with 500 nM of latrunculin A (Lat.A) and 5 μ M cytochalasin D (CD), which are both actin depolymerization agents, together with 20 μ M TAT, TAT-RasGAP₃₁₇₋₃₂₆ (TAT-P) and left untreated (Ctrl). Ten μ g of Triton-insoluble (F-actin containing) and Triton-soluble (G-actin containing) fractions were subjected to a Western blot directed against β -actin. The histogram shows the ratio between F-actin and G-actin.

B. U2OS cells were pre-treated for 1 hour with 50 nM jasplakinolide, 500 nM latrunculin A, 5 μ M cytochalasin D or were left untreated. They were then stimulated or not for 16 hours with 20 μ M TAT or TAT-RasGAP₃₁₇₋₃₂₆. A trypsin-mediated detachment assay was finally performed. Values too low to be seen on the figure graphs are shown literally.

C. An *in vitro* pyrene-actin polymerization assay was performed to evaluate the ability of RasGAP₃₁₇₋₃₂₆ to modulate actin polymerization by itself. Five minutes after the beginning of the experiment, 20 μ M RasGAP₃₁₇₋₃₂₆, 2 μ M jasplakinolide, 6 μ M latrunculin A or 6 μ M cytochalasin D were added to the actin-

containing buffer, followed 20 minutes later with the addition of the actin polymerization buffer. The graph shown is representative of 5 independent experiments.

Figure 5. TAT-RasGAP₃₁₇₋₃₂₆ does not require the Rho/ROCK axis.

A. U2OS cells were treated 16 hours with 20 μ M TAT, TAT-RasGAP₃₁₇₋₃₂₆ or left untreated and were then subjected to a RhoA activation assay (the statistical significance of the observed differences was assessed by one-way ANOVA).

B. U2OS cells were treated with the indicated combinations of 20 μ M TAT, 20 μ M TAT-RasGAP₃₁₇₋₃₂₆, 10 μ M of the Y-27632 ROCK inhibitor and 0.5 μ g/ml of the exoenzyme C3 transferase for 8 hours. The cells were then subjected to a trypsin-mediated detachment assay (graph on the upper left of the panel). The two pictures on the right highlight the phenotype difference between TAT-RasGAP₃₁₇₋₃₂₆⁻ and Y-27632-treated cells (scale bar: 50 μ m). A RhoA activation assay was performed to control the inhibitory activity of the C3 transferase (blot on the lower left of the panel). Values too low to be seen on the figure graphs are shown literally.

C. U2OS cells were pre-incubated 1 hour with 0.5 μ g/ml exoenzyme C3 transferase or left untreated (Control), then treated with 20 μ M TAT or TAT-RasGAP₃₁₇₋₃₂₆ for 12 additional hours. Bright field pictures are shown. Scale Bar: 50 μ m.

Figure 6. TAT-RasGAP₃₁₇₋₃₂₆ inhibits cell migration and invasion.

A. The indicated cell lines were subjected to wound-healing scratch assays. After wounding, the cells were left untreated or incubated 24 and 48 hours with 20 μ M TAT or TAT-RasGAP₃₁₇₋₃₂₆. Wound widths at the indicated time are reported in the graphs (n=4 independent experiments). Scale bar: 100 μ m.

B. 4T1 cells were cultured in the upper chamber of transwell plates and allowed to migrate through the Transwell filters for 24 hours in the absence (control) or in the presence of 20 μ M TAT or TAT-RasGAP₃₁₇₋₃₂₆. DMEM complemented (+) or not (-) with serum was added in the lower chamber. Quantitation was done as described in the methods. Three representative independent images are shown per condition.

C. MDA-MB-231 cells were allowed to invade the Matrigel matrix by following a serum gradient for 48 hours in presence of 20 μ M TAT, TAT-RasGAP₃₁₇₋₃₂₆. A negative control without serum in the lower chamber was also performed. The invading cells were then counted and expressed as the percentage of invading cells per transwell over the "control + serum" condition. Representative images are shown. Scale bar: 50 μ m.

Figure 7. DLC1 is required for TAT-RasGAP₃₁₇₋₃₂₆-mediated effects on adhesion and migration.

A. HEK 293T cells were transfected with the indicated combinations of plasmids. Two milligrams of cell lysates were immunoprecipitated using an anti-V5 antibody. Forty μ g of total lysates (T.L.) were also loaded. Western blotting against the HA and V5 tags was performed.

B. U2OS cells treated or not for 8 hours with 20 μ M TAT, TAT-RasGAP₃₁₇₋₃₂₆ or TAT-RasGAP₃₁₇₋₃₂₆ bearing the W317A mutation were subjected to a trypsin-based detachment assay.

C. Wild-type MEFs (WT) or DLC1^{-/-} MEFs treated for 8 hours with 20 μ M TAT, TAT-RasGAP₃₁₇₋₃₂₆ or left untreated were subjected to a trypsin-based detachment assays. Values too low to be seen on the figure graphs are shown literally.

D. WT or DLC1^{-/-} MEFs were treated with 20 μ M TAT, TAT-RasGAP₃₁₇₋₃₂₆ or left untreated. The cells were then subjected to wound-healing scratch assays for 48 hours. Scale bar: 100 μ m.

E. DLC1^{-/-} MEFs were co-transfected with a plasmid encoding GFP and with either a DLC1-encoding plasmid or with the empty pcDNA3 vector. The cells were then subjected to a 24 hour wound-healing scratch assays in the presence or in the absence of 20 μ M TAT or TAT-RasGAP₃₁₇₋₃₂₆. The migration was calculated as the number of GFP-positive cells that migrated through the initial wound made at 0 hour (yellow dotted lines). Scale bar: 100 μ m.

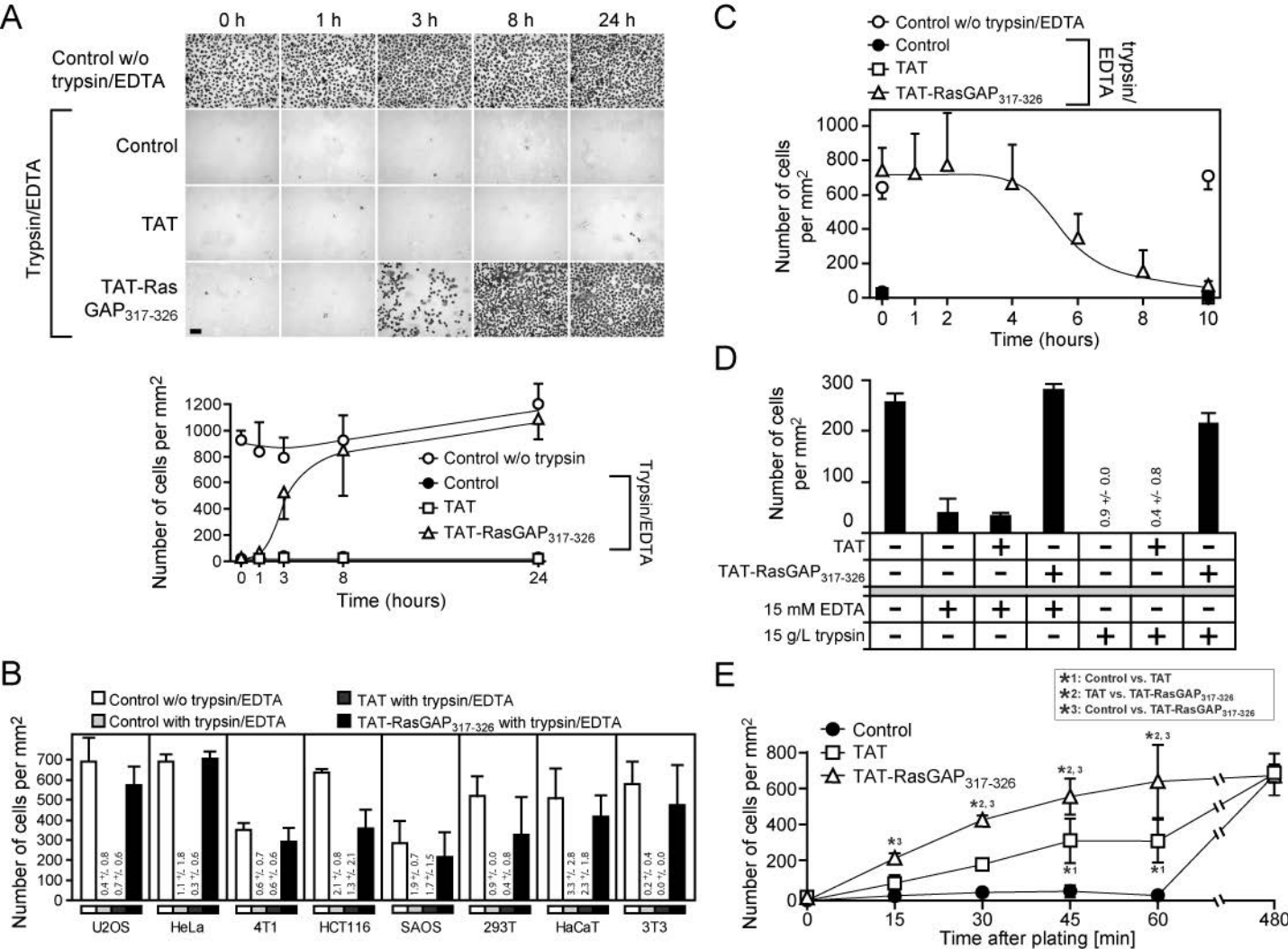


Figure 1

Strength of adhesion

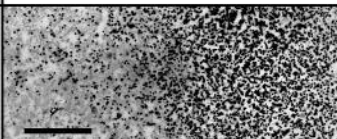
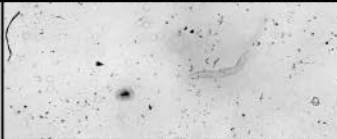
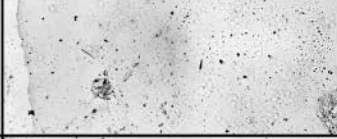
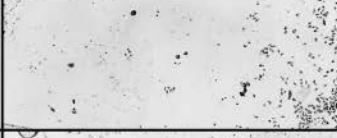
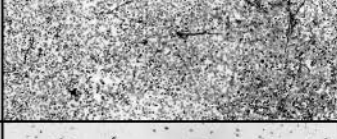
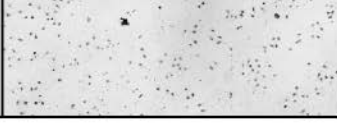
	flow [μ l/s]	time [min]	
Control	0	0	
	120	30	
	400	2	
TAT	120	30	
	400	2	
TAT-RasGAP ₃₁₇₋₃₂₆	120	30	
	400	2	

Figure 2

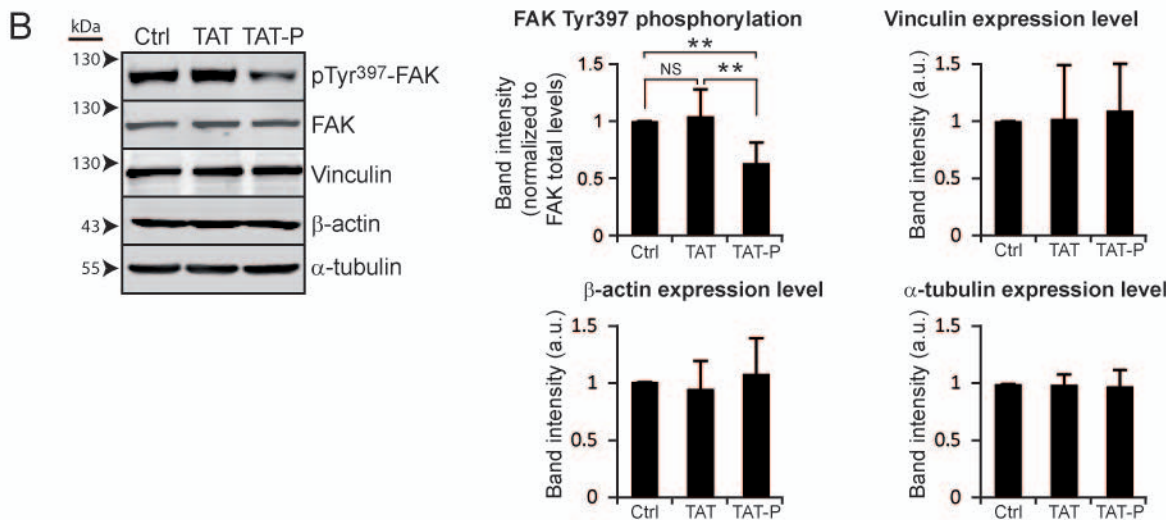
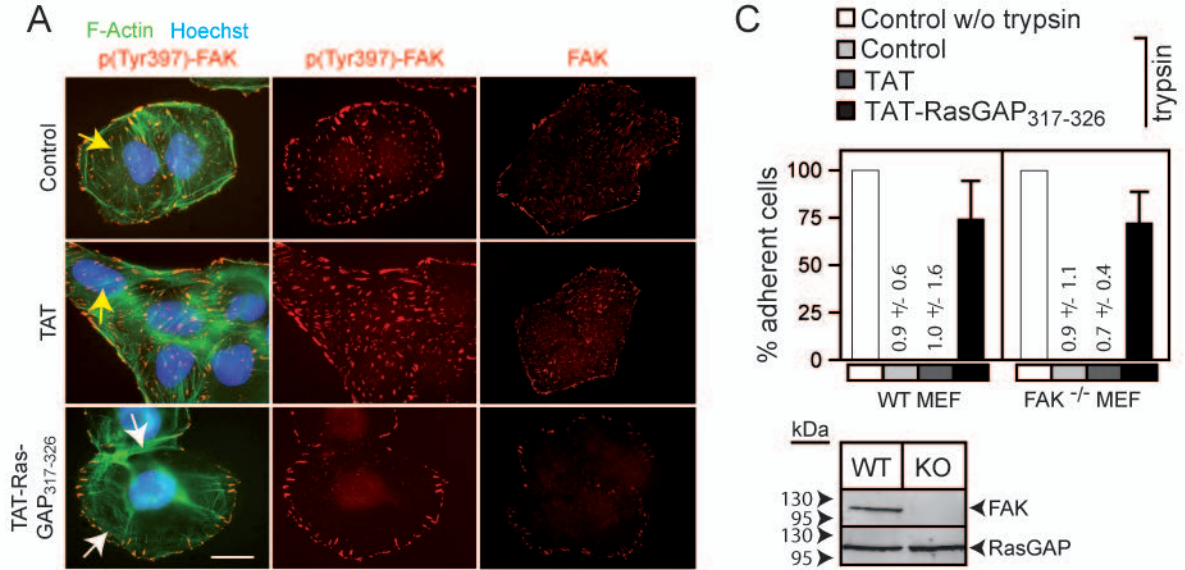


Figure 3

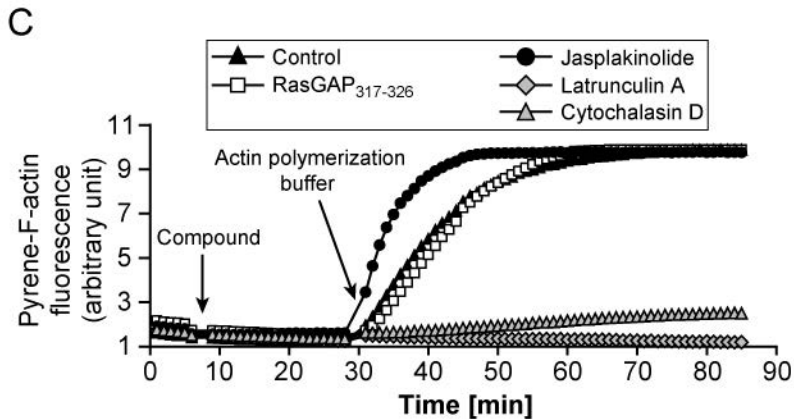
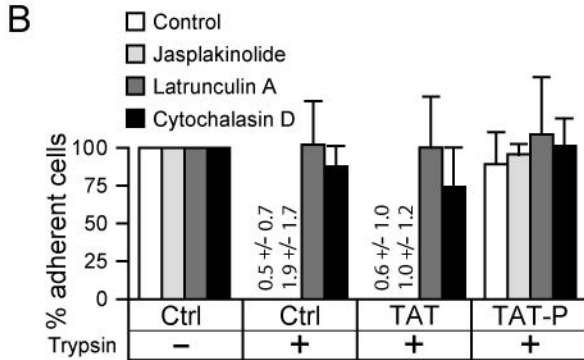
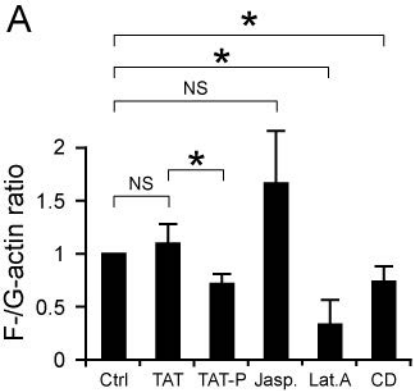


Figure 4

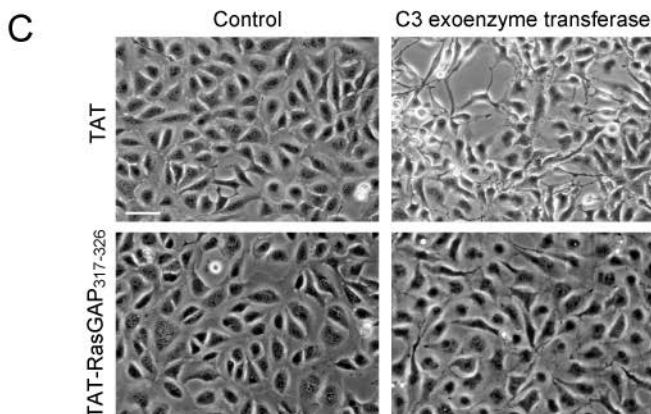
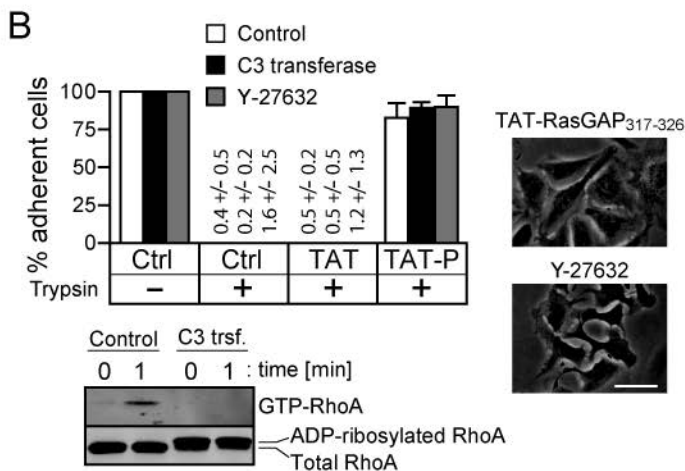
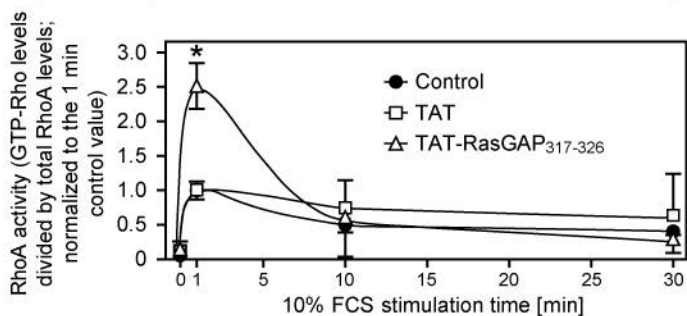
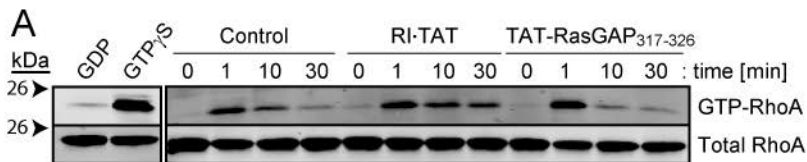


Figure 5

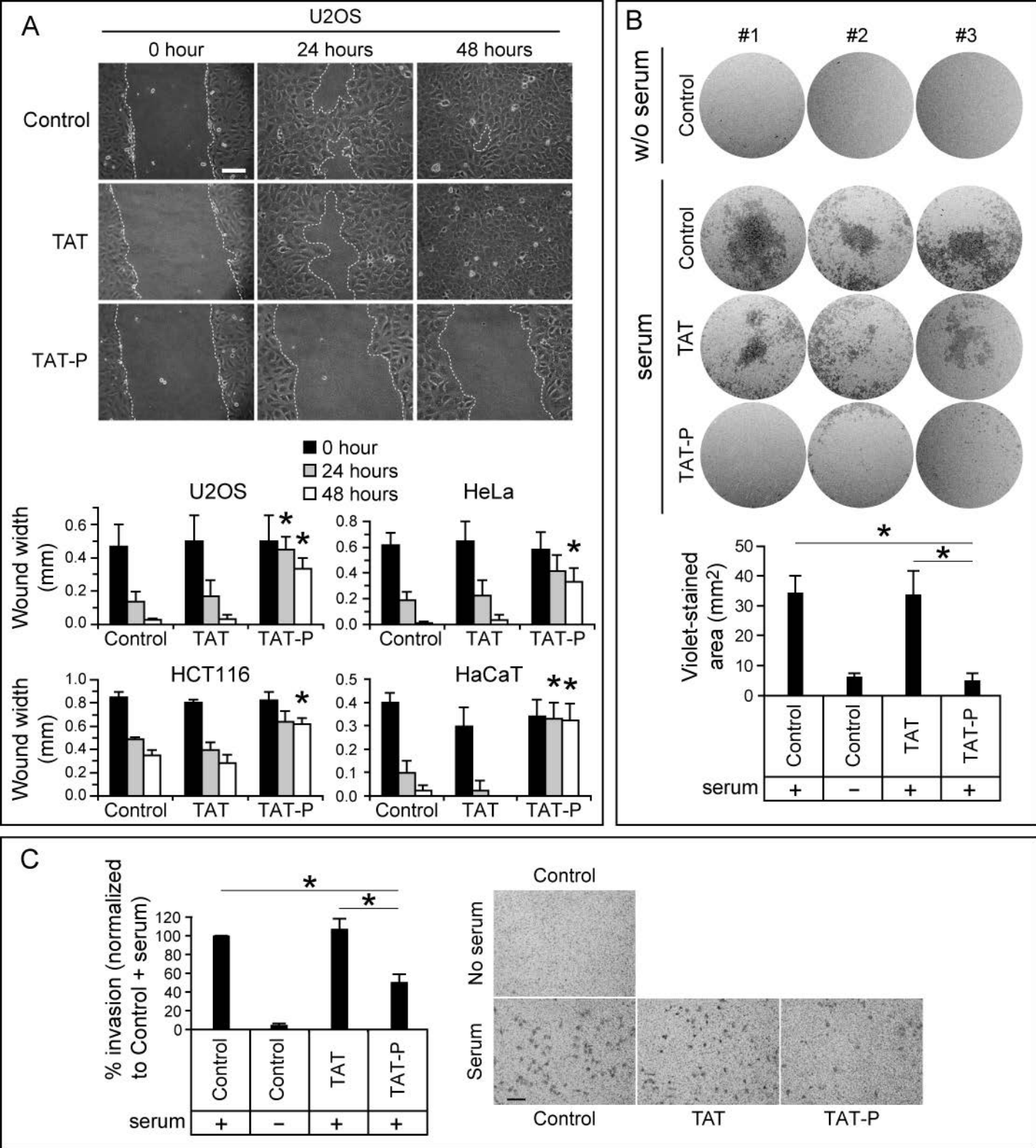


Figure 6

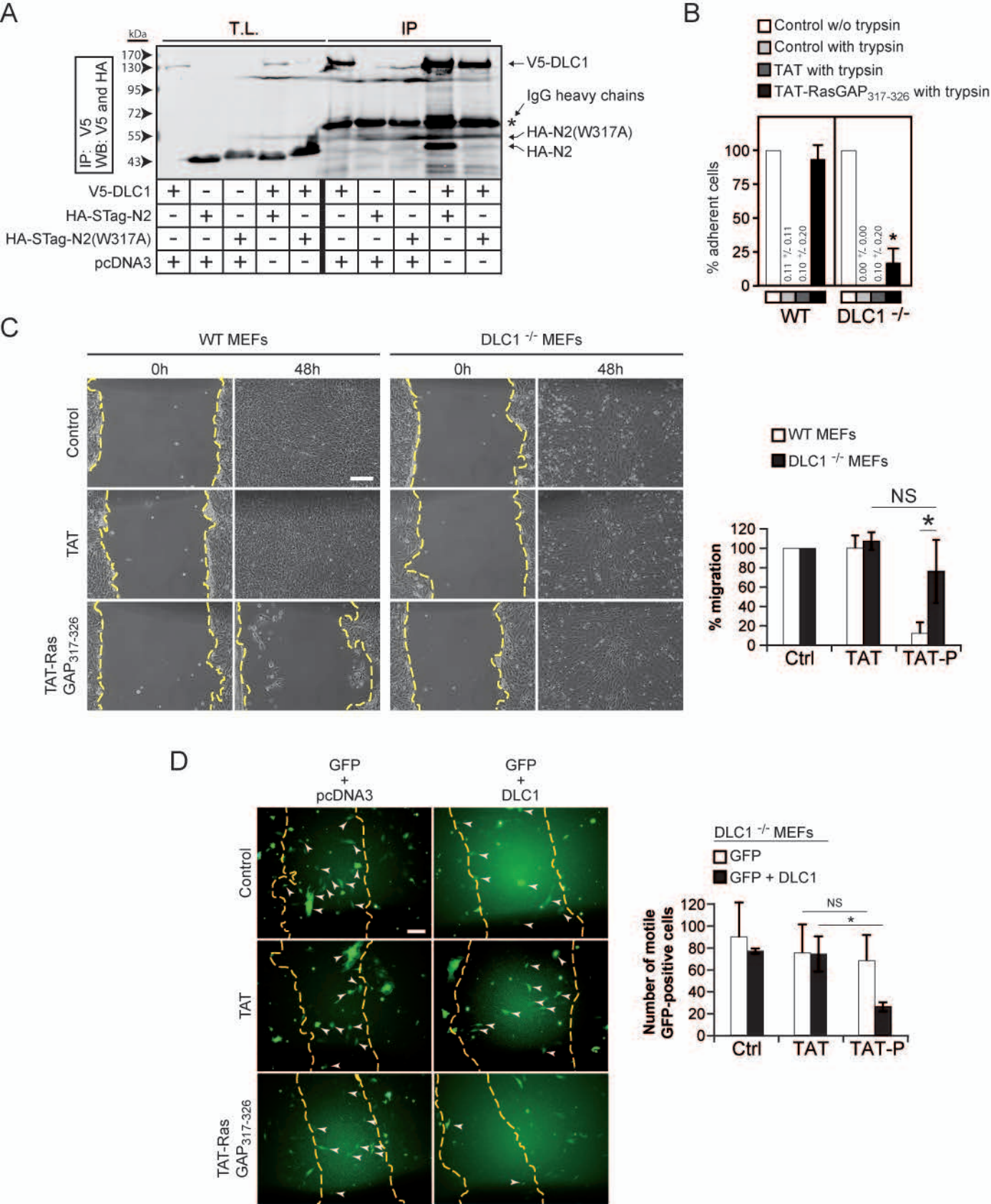


Figure 7

Figure S1

A

Adhesion rate

15 min

30 min

45 min

60 min

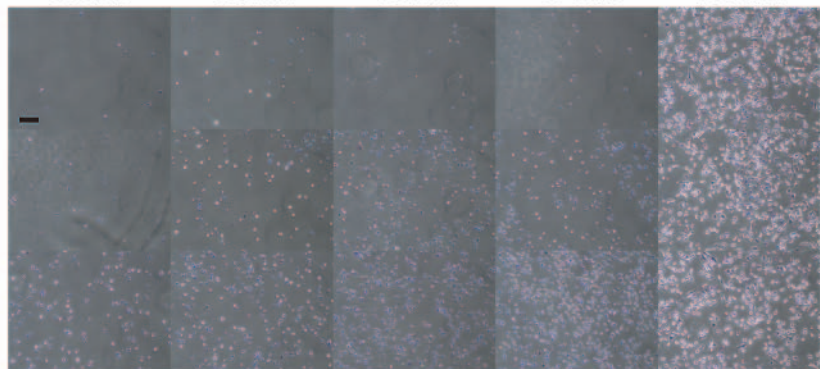
480 min

Control

TAT

TAT-Ras

GAP₃₁₇₋₃₂₆



Trypsin-mediated detachment

15 min

30 min

45 min

60 min

480 min

Control

TAT

TAT-Ras

GAP₃₁₇₋₃₂₆



B

Cell spreading

30 min after plating

Control

TAT

TAT-RasGAP₃₁₇₋₃₂₆



Figure S1. Kinetics of TAT-RasGAP₃₁₇₋₃₂₆-mediated adhesiveness increase.

A. Representative images of the adhesion assay performed in Figure 1E. Scale bar: 100 μ m.

B. Higher magnification of cells 30 minutes after plating. Scale bar: 40 μ m.

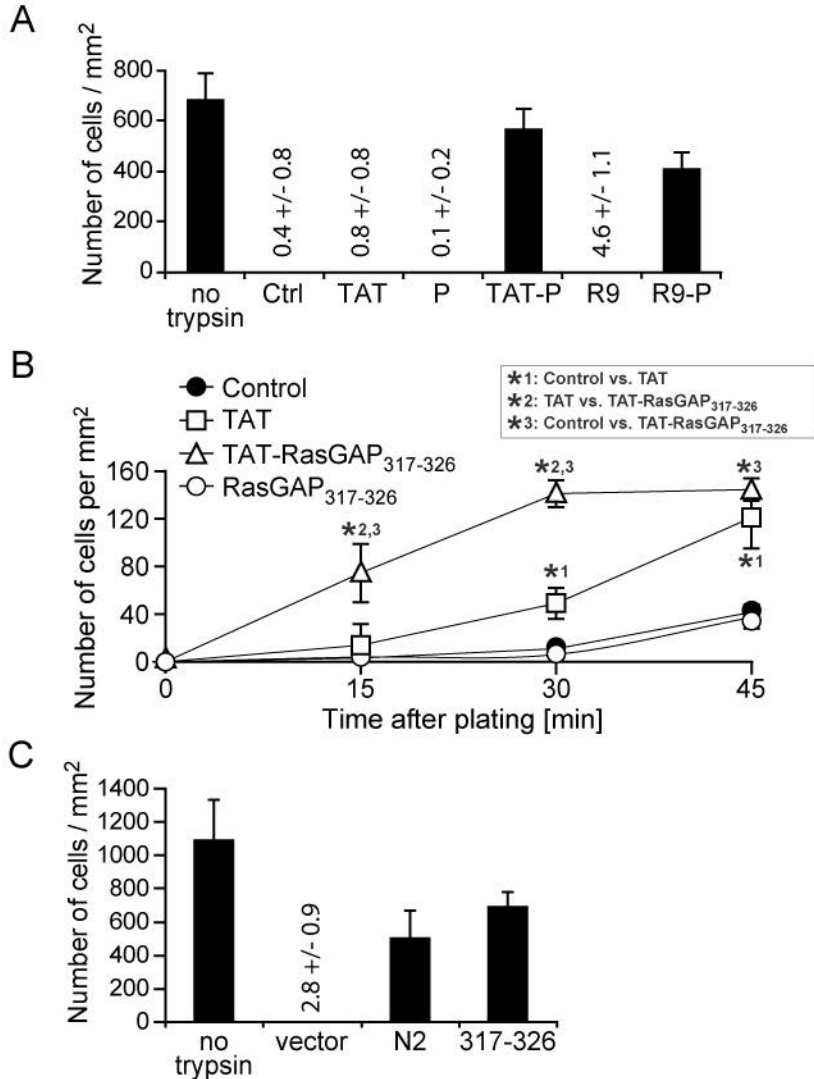


Figure S2. RasGAP₃₁₇₋₃₂₆ acts from inside cells.

A. U2OS cells were treated for 8 hours with 20 μ M TAT, 20 μ M RasGAP₃₁₇₋₃₂₆ (P), 20 μ M TAT-RasGAP₃₁₇₋₃₂₆ (TAT-P), 20 μ M R9, 20 μ M R9-RasGAP₃₁₇₋₃₂₆ (R9-P) or left untreated (Ctrl). A trypsin/EDTA-mediated detachment assay was then performed. A control without trypsin was also performed.

B. An adhesion assay was performed to assess the adhesion rate of U2OS cells in the presence of a RasGAP₃₁₇₋₃₂₆ peptide lacking the TAT cell permeable peptide. Treatment of cells with 20 μ M TAT-RasGAP₃₁₇₋₃₂₆ increased significantly the speed of adhesion compared to cells treated with 20 μ M TAT, 20 μ M RasGAP₃₁₇₋₃₂₆ or not treated. The statistical significance of the observed differences (asterisks) was assessed by one-way ANOVA.

C. HEK 293T cells were transfected with pcDNA3 (vector) or pcDNA3 encoding the HA-tagged forms of the N2 fragment of RasGAP (N2) or the 317-326 RasGAP sequence (317-326). A trypsin-mediated detachment assay was then performed but without tapping the plates. No trypsin, cells transfected with pcDNA3 that were not trypsinized.

Figure S3

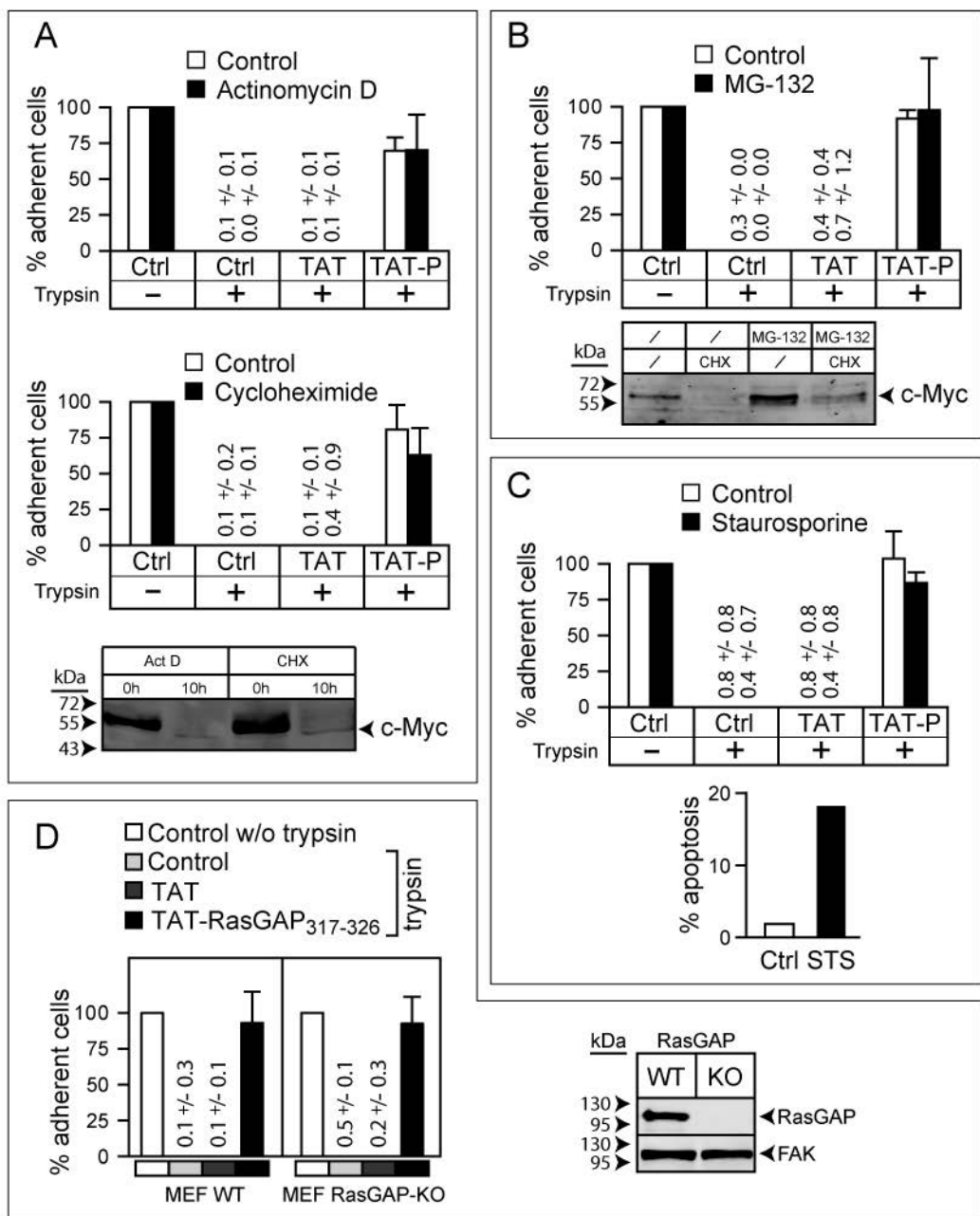


Figure S3. TAT-RasGAP₃₁₇₋₃₂₆ does not require transcription, translation, proteasome-mediated degradation, staurosporine-inhibitable kinases, and full-length RasGAP to increase adhesion.

A-B-C. U2OS cells were pre-incubated 2 hours with either 1 μ g/ml actinomycin D (Act D) or 30 μ g/ml cycloheximide (CHX) (panel A), with 10 μ M MG-132 for 16 hours (panel B), with 10 nM staurosporine (STS) for 16 hours (panel C), then treated 8 hours, in the presence of the inhibitors, with 20 μ M TAT (TAT), 20 μ M TAT-RasGAP₃₁₇₋₃₂₆ (TAT-P) or left untreated (Ctrl). The cells were then subjected to a trypsin-mediated detachment assay. The lower panels in A and B depict c-Myc expression levels after Act D, CHX and MG-132 treatments (25 μ g of loaded proteins). The activity of staurosporine was controlled by evaluating its capacity to induce apoptosis, determined by measuring the percentage of cells with pycnotic nuclei (panel C, lower graph).

D. Mouse embryonic fibroblasts (MEF) or RasGAP-knock-out MEF (KO) cells were treated for 8 hours with 20 μ M TAT, 20 μ M TAT-RasGAP₃₁₇₋₃₂₆ or left untreated. A trypsin-mediated detachment assay was performed as described for panel A-B. RasGAP expression was checked in wild-type and knock-out MEFs by immunoblotting (blot on the right-hand side of the panel).

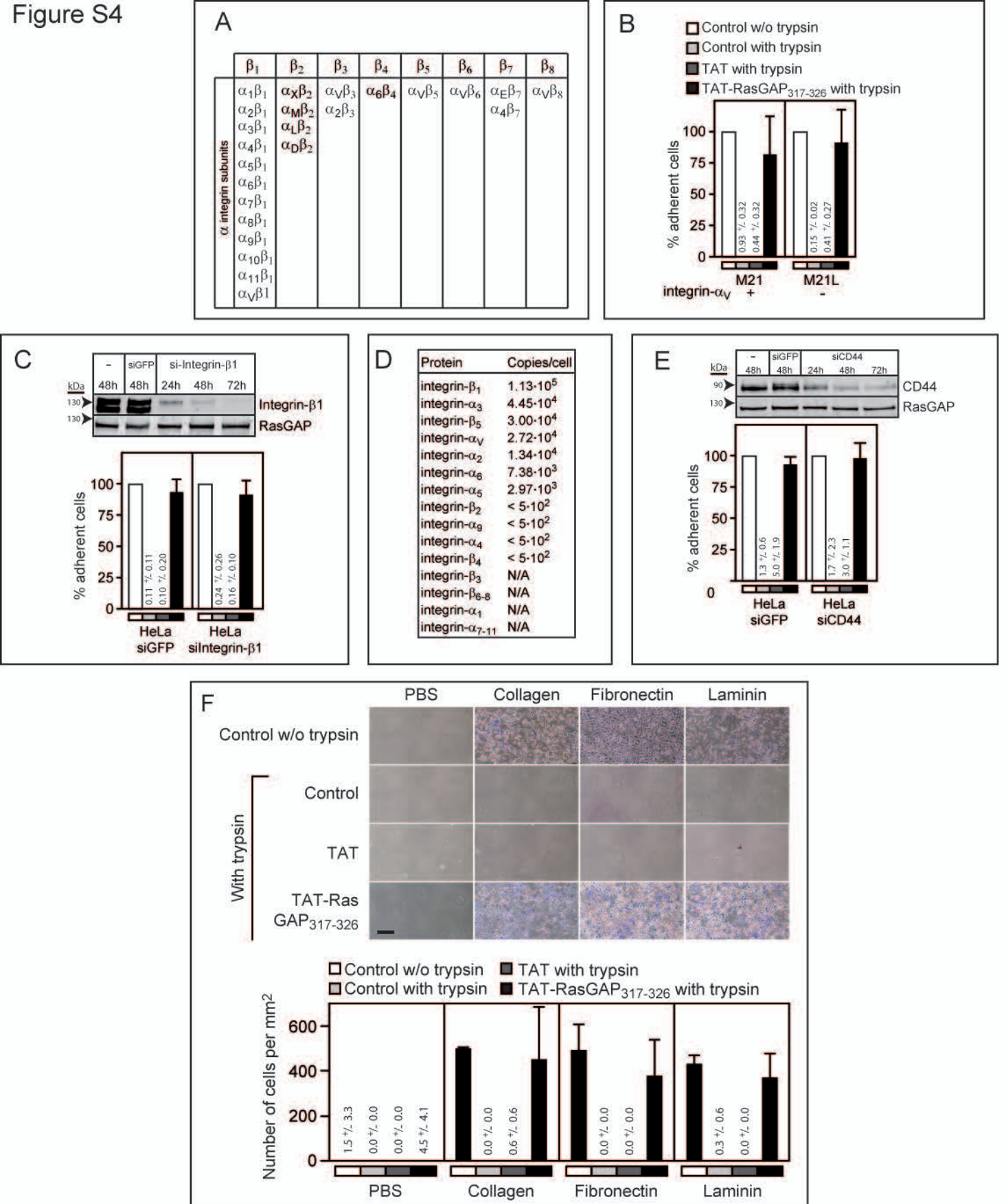


Figure S4. Integrins, CD44 and caspases are not required for TAT-RasGAP₃₁₇₋₃₂₆-mediated adhesion increase.

A. The twenty-four known integrin heterodimers are represented (8).

B. Wild-type (M21) or α_V -integrin-null (M21L) melanoma cells were treated 8 hours with 20 μ M TAT, 20 μ M TAT-RasGAP₃₁₇₋₃₂₆ or left untreated. The cells were then subjected to a trypsin-mediated detachment assay.

C. HeLa cells were transfected with siRNAs targeted against GFP (siGFP) or β_1 -integrin (siIntegrin- β_1). Forty-eight hours later, the cells were incubated 8 hours with 20 μ M TAT, 20 μ M TAT-RasGAP₃₁₇₋₃₂₆ or left untreated and were subjected to a trypsin-mediated detachment assay. The upper panel depicts the loss of β_1 -integrin expression after siRNA transfection.

D. Expression levels of the indicated integrin family members in U2OS cells [data taken from (9)].

E. CD44 was silenced in HeLa cells with siRNAs. Forty-eight hours later, the cells were incubated 8 hours with 20 μ M TAT, 20 μ M TAT-RasGAP₃₁₇₋₃₂₆ or left untreated. The cells were then subjected to a trypsin-mediated detachment assay. The upper panel depicts the loss of CD44 expression after siRNA transfection.

F. U2OS cells were grown overnight on bacteriological Petri dishes that had been coated beforehand with collagen, fibronectin or laminin. The cells were then treated or not with 20 μ M TAT or 20 μ M TAT-RasGAP₃₁₇₋₃₂₆ for 8 hours. A trypsin-based detachment assay was finally performed. Representative images of the cells remaining attached to the plates after trypsin treatment are shown. Scale bar: 100 μ m.

Figure S5

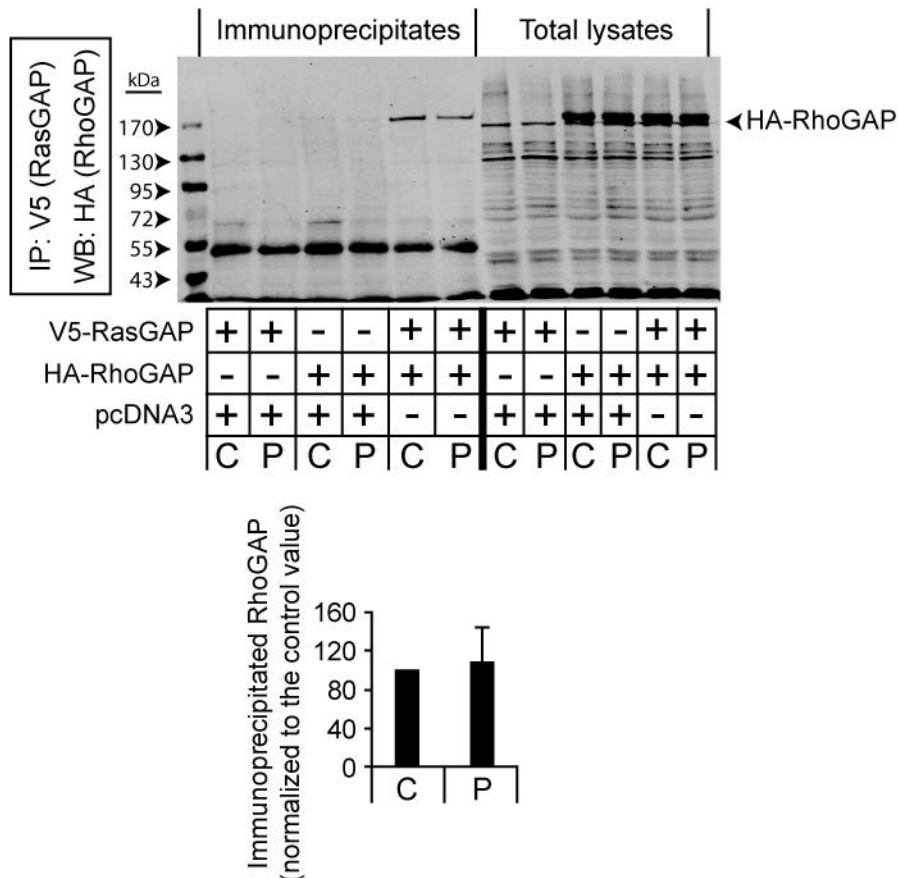


Figure S5. TAT-RasGAP₃₁₇₋₃₂₆ does not disrupt p120RasGAP:p190RhoGAP binding. HEK 293T cells were transfected with the indicated combinations plasmids encoding V5-RasGAP or HA-RhoGAP. Seven hundred μ g of lysates from cells treated with 20 μ M TAT-RasGAP₃₁₇₋₃₂₆ for 24 hours (P) or left untreated (C) were immuno-precipitated with an anti-V5 antibody to precipitate exogenous p120RasGAP. Western blot against the HA-tag was performed to detect pull-down p190RhoGAP. Forty μ g of total lysates were loaded as control. The graph represents the quantitation of the immuno-precipitated p190RhoGAP (normalized to the total lysate).

Figure S6

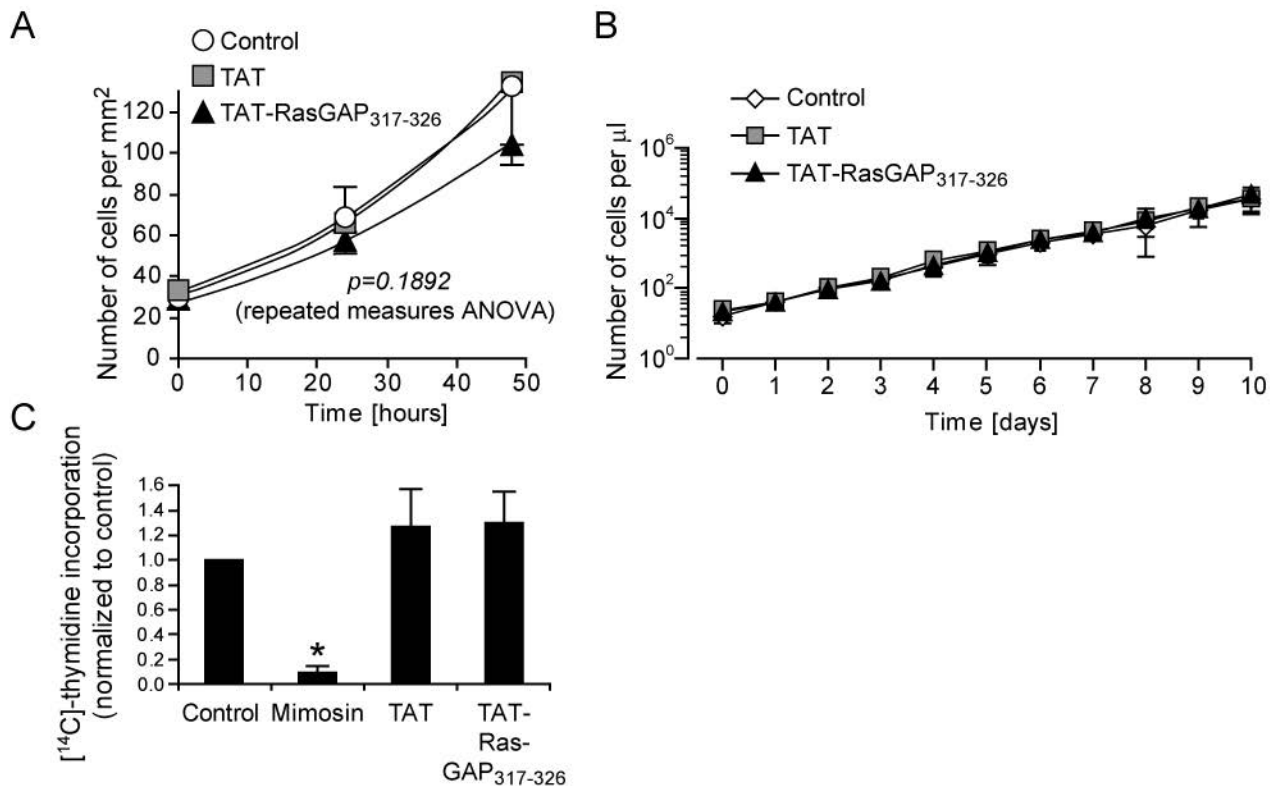


Figure S6. TAT-RasGAP₃₁₇₋₃₂₆ does not affect cell proliferation

A. U2OS cells were treated with 20 μ M TAT, 20 μ M TAT-RasGAP₃₁₇₋₃₂₆ or left untreated. The cell density was determined 0, 24 and 48 hours later. The curves were not found to differ significantly as assessed by repeated measures ANOVA.

B. Jurkat cells were treated with 20 μ M TAT, 20 μ M TAT-RasGAP₃₁₇₋₃₂₆ or left untreated, and were tested for their ability to proliferate in suspension for 10 days. The graph displays the number of cells per ml (cell splitting was performed when appropriate).

C. U2OS cells were treated 16 hours with 400 μ M mimosine, 20 μ M TAT, 20 μ M TAT-RasGAP₃₁₇₋₃₂₆ or left untreated, and were tested for their ability to incorporate radioactive thymidine during 2.5 hours. Mimosine significantly altered DNA synthesis, while TAT and TAT-RasGAP₃₁₇₋₃₂₆ did not.

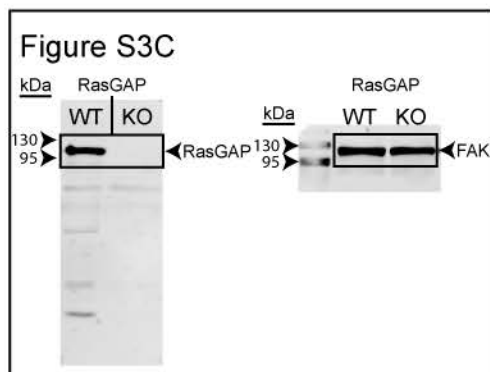
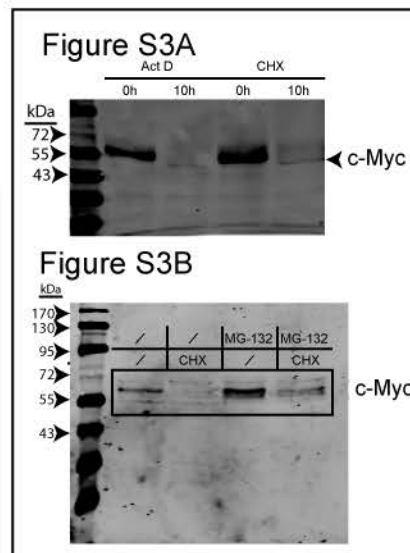
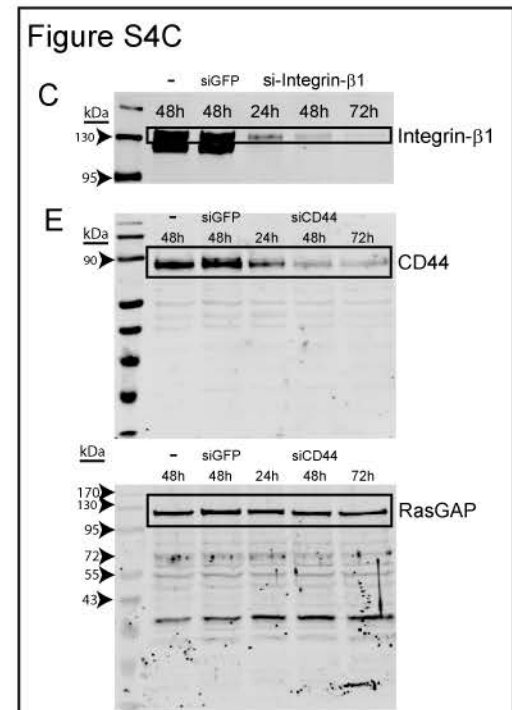
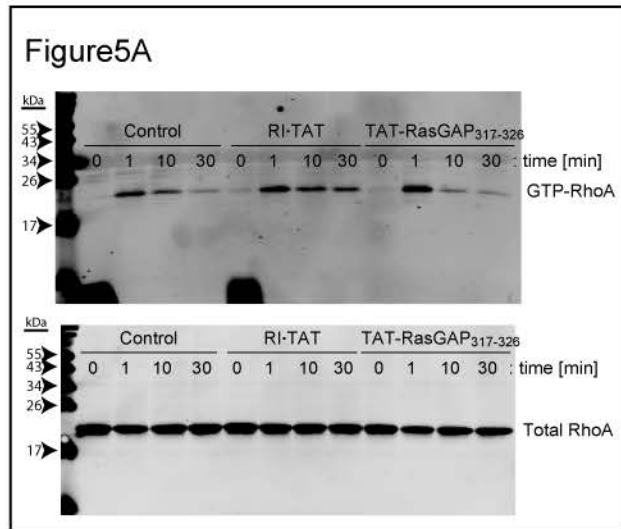
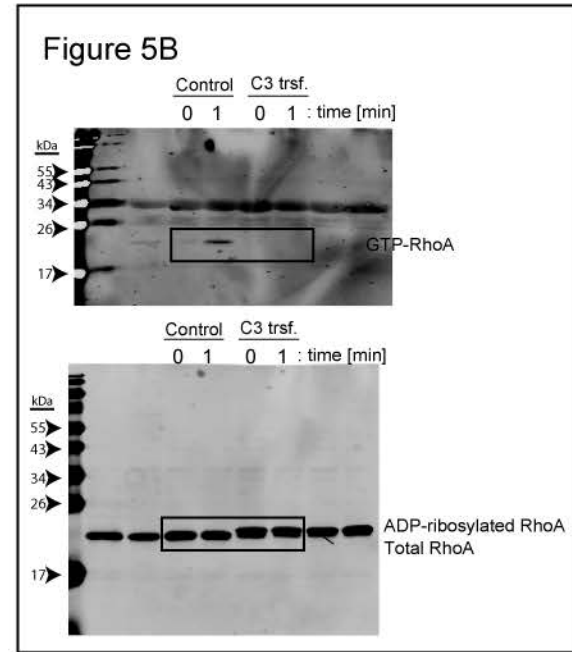
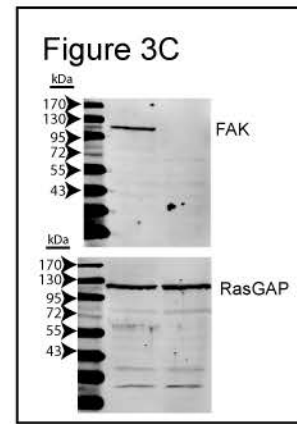
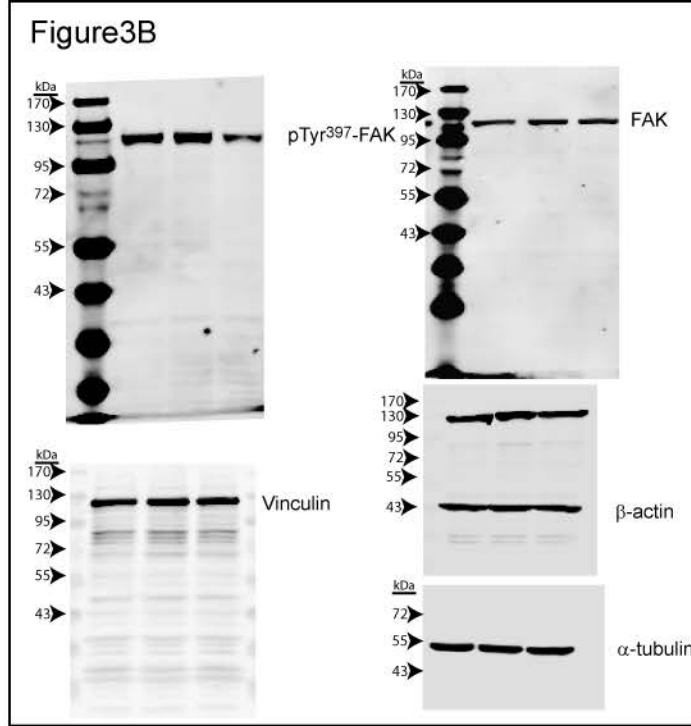


Figure S7. Original blots.
Blots that were cropped in the figures are displayed here in their original versions.

SUPPLEMENTARY MATERIAL AND METHODS

Antibodies

The following antibodies were used for Western blotting. Their reference, dilution and specific buffer ("milk" for 5% non-fat milk (in TBS [18 mM HCl, 130 mM NaCl, 20 mM Tris] containing 0.1% Tween (v/v)) or "BSA" for 5% BSA (in TBS containing 0.1% Tween)) are mentioned in parentheses. The primary antibodies used were anti-c-Myc (Cell Signaling; ref: 9402; 1:1000; BSA), anti-FAK (Cell Signaling; ref: 3285; 1:1000; BSA), anti-phospho-Tyr397-FAK (Cell Signaling; ref: 3283; 1:1000; BSA), anti-vinculin (Sigma-Aldrich; ref: V9131; 1:1000; milk), anti- β -actin (Chemicon International Inc; ref: MAB1501; 1:5000; milk), anti- α -tubulin (Serotec; ref: MCA77G; 1:1000; milk), anti-RasGAP directed at the SH3 domain (Enzo life sciences; ref: ALX-210-860-R100; 1:250; milk), anti-CD44 (Abcam; ref: 41478; 1:1000; milk), anti- β 1-integrin (BD Pharmingen; ref: 550531; 1:1000; milk), anti-V5 (Invitrogen; ref: 46-0705; 1:2500; milk) (also used for immunoprecipitation), anti-HA (Covence; ref: MMS-101r; 1:1000; milk), anti-RhoA (Cell Signaling; ref: 67B9; 1:1000; BSA). The secondary antibodies used were IRDye800-conjugated anti-mouse IgG (Rockland; ref: 610-132-121; 1:5000; milk), IRDye800-conjugated anti-rabbit IgG (Rockland; ref: 611-132-122; 1:5000; milk), AlexaFluor 680-conjugated anti-mouse IgG (Molecular Probes; ref: A21058; 1:5000; milk) or AlexaFluor 680-conjugated anti-rabbit IgG (Molecular Probes; ref: A21109; 1:5000; milk).

The following antibodies were used for immunocytochemistry. All the antibodies were diluted in DMEM containing 10% FBS. The primary antibodies used were anti-FAK (Cell Signaling; ref: 3285; 1:50), anti-phospho-Tyr397-FAK (Cell Signaling; ref: 3283; 1:50). The secondary antibody used was a donkey CyTM-anti-rabbit secondary antibody (Jackson ImmunoResearch; ref: 711-165-152; 1:500).

Chemicals

The following products were used in this study: actinomycin D (Calbiochem; ref: 114666), cycloheximide (Sigma-Aldrich; ref: C7698), MG-132 (Calbiochem; ref: 133407), staurosporin (Sigma Aldrich; ref: 200-664-3), latrunculin A (Adipogen; ref: AG-CN2-0027), jasplakinolide (Adipogen; ref: AG-CN2-0037),

cytochalasin D (Applichem; ref: A7641), Y-27632 (Alexis; ref: 270-333-M001), exoenzyme C3 transferase (Cytoskeleton; ref: CT04), mimosine (Sigma-Aldrich; ref: 500-44-7), Hoechst-33342 (Molecular Probes; ref: H1399) and AlexaFluor 488 phalloidin (Invitrogen; ref: A12379).

Plasmid description

The extension .dn3 and .prc indicate that the backbone plasmids are pcDNA3 (#1) and pRc/CMV from Invitrogen. The **pEGFP-C1** (#6) plasmid encodes the green fluorescent protein and is from Clontech. **V5-hRasGAP[3-1931].dn3** (#686) encodes a V5-tagged version of human RasGAP that lacks its first two methionine residues (to prevent potential internal translation events)¹. **HA-rRhoGAP.prc** (#196) encodes the HA-tagged form of rat p190RhoGAP¹. **HA-hRasGAP[158-455].dn3** (#145) previously called HA-N2.dn3², encodes the HA-tagged form of fragment N2. The **STag-HA-hRasGAP[158-455].dn3** (#644) plasmid encodes the Stag- and HA-tagged form of fragment N2. The STag was generated by PCR using oligonucleotide #678 [TAAGCAG (Feeder) AAGCTT (HindIII site) CTCGAG (XhoI site) CCACCATGGCG (including a start codon and alanine codon; the last nucleotide of the XhoI recognition site provides the G at the -6 Kozak position) AAA GAA ACC GCT GCT GCT AAA TTC GAA CGC CAG CAC ATG GAC AGC (STag) GGC TAC CCG TAC GAC GTG CCG (First 21 base pairs of fragment N2 (without the ATG))] and oligonucleotide #679 [GCA TTT AGG TGA CAC TAT AG: nucleotides 1018-999 of pcDNA3 (#1)]. The resulting 1057 base pair PCR fragment was cut with HindIII and subcloned into HA-hRasGAP[158-455].dn3 (#145) opened with the same enzyme. The **STag-HA-hRasGAP[158-455](W317A).dn3** (#793) plasmid encodes a Stag- and HA-tagged form of fragment N2 bearing a mutation of tryptophan 317 into an alanine residue (W317A). The template vector used for starting the mutagenesis is the Stag-HA-hRasGAP[158-455].dn3 plasmid (#644). Mutagenesis was performed using the mega-primer procedure³ as follows. (i) The W317A mutation was generated by PCR amplification of Stag-HA-hRasGAP[158-455].dn3 (#644) using oligonucleotide #978 [human RasGAP nucleotides 1052 to 1097 (NCBI entry M23379) except for nucleotides (underlined) that create a W317A mutation and a silent mutation generating a Bsu36I restriction site: GAA TTA GAA GAT GGA GCG (W317A) ATG TGG GTT ACA AAC C (N1-N2 of Bsu36I) TA AGG (N7 of Bsu36I) ACAGATG] and oligonucleotide #62 [TACCTAGCATGAACAGATTG (random sequence) AGGGGCAAACAACAGATG

(pcDNA3 nucleotides 1080-1063)]. (ii) The PCR product obtained in (i) was purified and elongated on the Stag-HA-hRasGAP[158-455].dn3 (#644) template. (iii) The PCR reaction was resumed after the addition of oligonucleotide #28 [TAATACGACTCACTATAGGGAGA (pcDNA3 sequence 863-885)] and oligonucleotide #70 [TACCTAGCATGAACAGATTG (same random sequence as in nucleotide #62)]. The PCR in (iii) was digested with BsiWI and NotI and ligated into plasmid STag-HA-hRasGAP[158-455].dn3 (#644) digested with the same enzymes. The **HA-hRasGAP[317-326].dn3** (#672) plasmid encodes the HA-tagged version of the RasGAP 317-326 sequence. The insert was created by annealing of oligonucleotide #736 [AATTC (cleaved EcoRI 5' end) GCCCC (Kozak) ATG GGC TAC CCG TAC GAC GTG CCG GAC TAC GCT TCT (HA tag) TGG ATG TGG GTT ACA AAT TTA AGA ACA GAT (RasGAP₃₁₇₋₃₂₆) TAG (Stop) G (cleaved BamHI 3' end)] and oligonucleotide #737 [GATCC (cleaved BamHI 5' end) CTA (stop) ATC TGT TCT TAA ATT TGT AAC CCA CAT CCA (RasGAP₃₂₆₋₃₁₇) AGA AGC GTA GTC CGG CAC GTC GTA CGG GTA GCC CAT (HA Tag) GGGGC (Kozak) G (cleaved EcoRI 3' end)]. The annealed oligonucleotides were inserted into pcDNA3 opened with BamHI and EcoRI. The **mDLC1[1-1092].pSK** plasmid (#789) encodes the *Mus musculus* DLC1 (deleted in liver cancer-1) transcript variant 2 (NM_015802.3), a gift from Dr. Nicholas C. Popescu (National Cancer Institute, Bethesda, US). This plasmid was obtained by subcloning the 3.3 kb cDNA of mouse DLC1 into a the pBluescript SK(+) vector using the Not and XhoI restriction enzymes. The **mDLC1[1-1092].dn3** (#790) plasmid encodes the same version of DLC1 under the control of a CMV promoter. The 3.3 kb fragment DLC1 cDNA fragment was excised from plasmid mDLC1[1-1092].pSK (#789) using NotI and XhoI and subcloned into pcDNA3 (#1) opened with the same enzymes. The **V5-mDLC1[1-1092].dn3** (#791) plasmid encodes the V5-tagged version of the DLC1 construct. It was generated by PCR amplification of mDLC1[1-1092].dn3 plasmid (#790) with oligonucleotide #975 [GGTGGT (feeder) GCGGCCGC (NotI site) GCCACC (Kozak) ATG (start) GGA AAA CCA ATA CCA AAT CCA CTA CTA GGC CTA GAC AGT ACA (V5-tag) ATC CTA ACA CAA ATT GAA GCC AAG (nucleotides 376-399 of mouse DLC1 transcript variant 2; NM_015802.3)] and oligonucleotide #976 [TTGTTACAGGTGCTGAGGCT (nucleotides 1352-1333 of mouse DLC1 transcript variant 2; NM_015802.3)]. The resulting 1013 base pair fragment was cut with NotI and BstEII and subcloned into mDLC1[1-1092].dn3 (#790) opened with the same enzymes.

Giemsa staining

Cells were washed once in PBS and air-dried overnight at room temperature. The next day, they were incubated 10 minutes in 100% ethanol and air-dried for 1 hour at room temperature. They were then colored with 2 ml of a Giemsa stain solution (4 mg/ml in methanol; Sigma-Aldrich; ref: G3032) per 3.5 cm plates (or 10 ml for 8.4 cm plates) for 45 minutes. The Giemsa solution was then discarded and the plates were immersed in a 5 liter becher containing tap water for 10 minutes. The water was then replaced with fresh water and this procedure was repeated until the background staining has been washed away, revealing the stained cells. The plates were then air-dried and kept at room temperature until analysis.

Flow-mediated detachment assay

HeLa cells were seeded on 20 mm coverslips coated with 0.1% gelatin (in PBS). The cells were then treated with 20 μ M TAT, 20 μ M TAT-RasGAP₃₁₇₋₃₂₆ for 8 hours or were left untreated. The coverslips were then washed in PBS and mounted in a home-made ovoid flow-chamber and the cells were subjected to different intensities of PBS flows. The 120 μ l/s flow was reached using a perfusion hanged 2.2 m above the flow chamber and the 400 μ l/s flow was reached by manual PBS injection using a syringe. After the assay, the undetached cells were colored with the Giemsa stain and pictures were taken.

Immunocytochemistry

U2OS cells were grown overnight on coverslips, and then treated as described in the figures. The immunocytochemistry was performed as described earlier⁴. Prior to antibody incubation, the cells were incubated 20 minutes in PBS containing 1.65 μ M Alexa Fluor 488 phalloidin (Invitrogen). Images were taken with a Zeiss Axioplan 2 imaging microscope and were similarly treated for their intensities and contrasts using Adobe Photoshop CS5.

Immunoprecipitation

Transfected 293T cells were lysed in 1% NP-40 lysis buffer. The amount of protein extract used for immunoprecipitation is indicated in the figures. The immunoprecipitation was performed using the

Dynabeads Protein G technology according to the manufacturer's instructions (Novex) and subjected to Western blotting.

siRNA-mediated gene silencing

The silencing was performed as follows: one hundred fifty thousand HeLa cells were cultured overnight in 3.5 cm plates in DMEM complemented with 10% FBS. The day after, the siRNA (Microsynth, Switzerland) were transfected using Lipofectamine™ 2000 (Invitrogen, ref: 11668-019) according to the manufacturer's instructions. Two hundred pmol of siRNA and 4 µl of Lipofectamine were used per well. The cells were transfected for the indicated period of time and followed by the indicated assays. The silencing was performed using the following siRNAs: β1-Integrin (5'-dTdT-AAU GUA ACC AAC CGU AGC ATT-dTdT-3'), CD44 (5'-dTdT-UUC CAG AAU GGC UGA UCA U-dTdT-3').

Extracellular matrix coating

Collagen was purified as previously described⁵. Two hundred µl drops of PBS or of the different extracellular matrix components [25 µg/ml fibronectin (BD Biosciences; ref: 354008), 50 µg/ml laminin (Boehringer Mannheim; ref: 1243217) and 3.9 mg/ml self-purified collagen] were laid on the surface of 9.2 cm bacteriologic Petri dishes (Sarstedt; ref: 82.1473) for 4 hours. These drops were then aspirated and the coated regions were washed with 200 µl PBS drops, and then aspirated again. Cells were then grown on these coated dishes as mentioned above.

Actin assays: F-actin/G-actin ratio measurement and pyrene-actin *in vitro* polymerization assay

F- and G-actin were purified as previously reported⁶ and the Triton-insoluble fractions (F-actin containing fractions) were washed once in lysis buffer and dissolved in 1% SDS buffer for 10 minutes at 96°C.

Actin *in vitro* polymerization was carried out using a kit purchased from Cytoskeleton (Denver; CO; USA). Briefly, One hundred µl of 2.38 µM rabbit skeletal muscle pyrene-G-actin (100 µg/ml) were added per well of a 96-well plate (Costar; ref: 07-200-590). After 355 nm wavelength excitation, the fluorescence emitted at 410 nm was measured every minute for the whole duration of the experiment. Five minutes after having started the recording, the actin mix was treated with 20 µM RasGAP₃₁₇₋₃₂₆, 2 µM jasplakinolide, 6 µM

latrunculin A or 6 μ M cytochalasin D (so that the compound volume corresponds to 2 μ l) and the measurement went on. Twenty minutes after compound incubation, ten μ l actin polymerization buffer from the kit were added to the mix and the measuring went on until the end of the experiment.

RhoA activation pull-down assay

The cellular level of GTP-loaded RhoA was determined as previously reported ⁷. U2OS cells were starved overnight in DMEM without serum in combination with 20 μ M TAT, 20 μ M TAT-RasGAP₃₁₇₋₃₂₆ or without treatment. The cells were then stimulated with DMEM complemented with 10% serum as indicated in the figures and processed as reported ⁷.

Wound-healing scratch assay

Confluent cells were wounded with a tip. The cells were then washed once with PBS and incubated in fresh medium in the conditions indicated in the figures. Pictures of the plates were taken just after wounding (0 hour) and at the indicated times. The same five fields per wound were photographed at each time point. The results were either reported as wound widths measured as described earlier ⁸. Alternatively, the 48 hour wound area was subtracted from the 0 hour wound area (quantitated using ImageJ) and expressed as a percentage of the untreated condition. Time-lapse microscopy was performed during 48 hours by taking brightfield snapshots every 5 minutes.

Transwell migration and invasion assay

After migration or invasion of cells into the filters of the Transwells, the cells that did not migrate or invade were removed by scraping with a cotton swab. The cells remaining within the filter were fixed in 4% paraformaldehyde for 10 minutes, rinsed 3 times in sterile water, stained with 0.5% (w/v) crystal violet (Acros, ref: 548-62-9) in 25% methanol (v/v) for 10 minutes, and then rinsed again 5 times in water. The quantitation of the violet area was done using the Adobe Photoshop software (Creative Suite 3) as follows. Pictures of the filters were taken at the same magnification and with the same luminosity condition using a stereoscopic zoom microscope (Nikon SMZ1000) equipped with a digital camera (Nikon DS-L2). The surface occupied by the cells, i.e. the violet-stained surface, was measured as follows. The Adobe

Photoshop software (Creative Suite 3) was used to draw a circle positioned on the center of the filter in the image. The diameter of the circle was set to 3/4 of the diameter of the actual filter (this ensures that cells close the walls of the wells, which are not efficiently removed with the cotton swab, do not artefactually alter the results). The magic wand tool was used to select the violet area and the tolerance was adjusted for each picture in order to discriminate the violet area from the non-stained area. The number of pixels of the violet area was determined (from the histogram window in Photoshop) and converted in mm^2 (the area of the circle corresponds to 79'868 pixels and 86.5 mm^2).

Cell density measurement

A one cm^2 grid was drawn on the bottom of 3.5 cm plates. Thirty thousand U2OS cells were seeded in those plates and cultured overnight. The cells were then treated as indicated in the figures. The number of cells within the one cm^2 square was determined at the time of treatment initiation and on the next two consecutive days. Cell density was expressed as number of cells per mm^2 . For Jurkat cell proliferation measurement, one hundred thousand cells were diluted in 5 ml RPMI supplemented with 10% FBS, in 3.5 cm plates. The cells were directly treated with 20 μM TAT, 20 μM TAT-RasGAP₃₁₇₋₃₂₆ or left untreated and cell density assessed using a Neubauer counting chamber.

Radioactive thymidine incorporation assay

U2OS cells were cultured and treated 16 hours with 400 μM Mimosin, 20 μM TAT, 20 μM TAT-RasGAP₃₁₇₋₃₂₆ or left untreated. [¹⁴C]-thymidine (0.01 μCi per well) (Perkin Elmer; ref: NEC1560110UC) was then added for 2.5 hours. Each well was washed four times with PBS and the cells were lysed in RIPA, spotted on glass microfiber filters (Whatman; ref: 10370018) and dried for 30 minutes. These filters were subsequently soaked into four different baths in the following order: (1) 10% TCA (trichloroacetic acid; Sigma; ref: 33731), (2) 5% TCA, (3) 50% ethanol + 50% ether and (4) 100% ether, and were dried 1 hour in scintillation vials. Each filter was then solubilized and beta particle emission was measured for 10 minutes. These emission values were normalized to the amount of proteins in the samples and further normalized to the non-treated control.

References

- 1 Annibaldi A, Dousse A, Martin S, Tazi J, and Widmann C. Revisiting G3BP1 as a RasGAP binding protein: sensitization of tumor cells to chemotherapy by the RasGAP 317-326 sequence does not involve G3BP1. *PLoS One* 2011; **12**: e29024
- 2 Yang JY and Widmann C. Antiapoptotic signaling generated by caspase-induced cleavage of RasGAP. *Mol Cell Biol* 2001; **16**: 5346-5358
- 3 Nelson RM and Long GL. A general method of site-specific mutagenesis using a modification of the *Thermus aquaticus* polymerase chain reaction. *Anal Biochem* 1989; **1**: 147-151
- 4 Annibaldi A, Michod D, Vanetta L, Cruchet S, Nicod P, Dubuis G *et al.* Role of the sub-cellular localization of RasGAP fragment N2 for its ability to sensitize cancer cells to genotoxin-induced apoptosis. *Exp Cell Res* 2009; **12**: 2081-2091
- 5 Brekhman V and Neufeld G. A novel asymmetric 3D in-vitro assay for the study of tumor cell invasion. *BMC Cancer* 2009; 415
- 6 Ueda H, Saga S, Shinohara H, Morishita R, Kato K, and Asano T. Association of the gamma12 subunit of G proteins with actin filaments. *J Cell Sci* 1997; **Pt 13**: 1503-1511
- 7 Ren XD and Schwartz MA. Determination of GTP loading on Rho. *Methods Enzymol* 2000; **325**: 264-272
- 8 Bulat N, Waeber G, and Widmann C. LDLs stimulate p38 MAPKs and wound healing through SR-BI independently of Ras and PI3 kinase. *J Lipid Res* 2009; **1**: 81-89
- 9 Michod D, Yang JY, Chen J, Bonny C, and Widmann C. A RasGAP-derived cell permeable peptide potently enhances genotoxin-induced cytotoxicity in tumor cells. *Oncogene* 2004; **55**: 8971-8978
- 10 Byron A, Morgan MR, and Humphries MJ. Adhesion signalling complexes. *Curr Biol* 2010; **24**: R1063-R1067
- 11 Beck M, Schmidt A, Malmstroem J, Claassen M, Ori A, Szymborska A *et al.* The quantitative proteome of a human cell line. *Mol Syst Biol* 2011; **7**: 549

Supplementary movie. TAT-RasGAP₃₁₇₋₃₂₆ inhibits cell migration

This movie displays a time-lapse recording of a wound healing scratch assay. U2OS cells were treated as indicated in the methods with 20 μ M TAT, 20 μ M TAT-RasGAP₃₁₇₋₃₂₆ or left untreated (control). Bright field pictures were taken every 5 minutes during 48 hours using a Zeiss LSM 710 NLO microscope equipped with a 10x objective. The cells were maintained at 5% CO₂ and 37°C for the whole duration of the experiment. The movie was then generated using the Metamorph software.